

Final design review (FDR)

RC Delivery Aircraft

Col. Pollo J. Rosso

Presented to the
University of California, San Diego
Department of Mechanical and Aerospace Engineering

MAE 155B

June 11th, 2025

Prepared by:

Team 3 MJ⁵

Jeffrey Denenberg, Jeffrey Bratman, Johnpierre Khachi,
Mark Gabriel Samac, Justin Rector, Joseph Tuazon

Table of Contents

Table of Contents.....	2
Figures & Tables.....	3
Nomenclature.....	5
1. Executive Summary.....	7
2. Introduction.....	9
3. Concept of Operations.....	9
3.1 Requirements and Constraints.....	9
3.2 Operations and Mission Profile.....	9
4. Sizing Analysis.....	10
4.1 Scoring Function.....	10
5. Configuration and Concept Design.....	11
5.1 Wing Design.....	11
5.2 Fuselage Structure.....	12
5.3 Landing Gear Choice.....	13
5.4 Payload Drop-off Mechanism.....	13
6. Aerodynamics.....	14
6.1 Assumptions.....	14
6.2 Airfoil Selection.....	14
6.3 Drag Buildup.....	15
7. Performance.....	16
7.1 Takeoff.....	16
7.2 Cruise.....	17
7.3 Maneuvering and Climb.....	17
8. Propulsion.....	18
8.1 Propulsion System Design.....	18
9. Weights and Balances.....	19
9.1 Weight Breakdown.....	19
9.2 Tail Sizing and Configuration.....	19
9.3 Control Surfaces.....	20
9.4 Static Stability.....	20
10. Completed Structural Framework.....	21
10.1 Fuselage.....	21
10.2 Wing.....	21
10.3 Horizontal and Vertical Tail.....	22
10.4 Nose and Propulsion System.....	22
10.5 Weight Payload.....	22
10.6 Volume Payload Delivery.....	23
10.7 Landing Gears.....	23
10.8 Control System\.....	23

11. Post Maiden Flight Alterations.....	24
12. Conclusion.....	24
References.....	25
Appendices.....	26
Appendix A - Figures.....	26
Appendix B - Equations.....	41
Appendix C - Tables.....	44

Figures & Tables

Table 1.1: Aircraft Requirements and Specifications supervised in MAE 155B Course.....	8
Figure 1.2: Cross sectional view of the aircraft.....	9
Table 2.2: Measures of Merit.....	10
Table 3.1: Targets and Constraints for a radio-powered aircraft.....	10
Table 3.2: The two missions of the aircraft and corresponding descriptions.....	11
Table 4.1: The J gain [\\$] per unit increase of a payload parameter, while keeping the other fixed.....	12
Figure 5.1: The skeletal wing structure design with wooden rib and spars, along with aileron.....	13
Figure 5.2: The CAD skeletal structure of the aircraft fuselage.....	13
Figure 5.3: The two proposed mechanisms for two-door opening and closing, gear-driven (left) and lever (right).....	14
Table 6.1: Main wing dimensions.....	15
Figure 6.1: Selected Airfoils 2-D Aerodynamic Analysis at $Re = 500,000$ and cruise speed of 25 m/s. Data imported from XFOIL. Lift Coefficient (top) and Drag Coefficient (bottom) vs Angle of Attack. Stall Angle of Attack at 13.25°	16
Table 6.2: Major Aerodynamic Parameters of selected airfoil, NACA 4412.....	16
Figure 6.2: 2-D and 3-D comparison. Lift coefficient with CL_{max} at 13.25° stall angle of attack (top); Drag coefficient vs angle of attack, 3-D includes the drag build-up for wing, fuselage, tails, propeller and landing gear. (bottom).....	17
Figure 7.1: Thrust required for steady level flight given different cruise velocities.....	18
Figure 7.2: T/W vs Wing loading at set performance and aerodynamic design parameters.....	19
Table 8.1: Propulsion Key Parameters comparison between 9x6E and 8x6E.....	19
Figure 9.1: Breakdown of Aircraft Weight and Material Composition.....	20
Table 9.1: Tail Sizing Dimensions.....	21
Table 9.2: Control Surface Sizing.....	21
Table 9.2: Aerodynamic stability results.....	22
Figure A.5.1: The landing gear configuration (Tail dragger).....	28
Figure A.6.1: K" estimation from the 2-D aerodynamic data for 3-D aerodynamic data calculations in Figure 6.2.....	29
Figure A.6.2: Other 2-D aerodynamic data for selected airfoils at $Re = 500,000$. Data collected from	

XFOIL.....	29
Figure A.7.1: The Graphical User Interface (GUI) of takeoff distance and stall speed calculations using MATLAB.....	30
Figure A.7.2: Top View of Mission Bay Runway with approximate total runway distance (80m) using ArduPilot Mission Planner Software.....	30
Figure A.8.1: Efficiency of different propellers as a function of advance ratio.....	31
Figure A.8.1: Power coefficient of different propellers as a function of advance ratio.....	31
Figure A.8.2: Torque coefficient of different propellers as a function of advance ratio.....	32
Figure A.8.3: Thrust coefficient of different propellers as a function of advance ratio.....	32
Figure A.9.1: Image of table 6.4 from Raymer [1] textbook that lists typical Tail Volume Coefficients.	
33	
Figure A.9.2: Plots of different dd vs r coefficient at varying taper, m coefficient, and aspect ratio..	34
Figure A.10.1.1: Top view of electronics bay showing the supporting brace for the main landing gear..	
35	
Figure A.10.1.2: Servo wiring in the fuselage.....	35
Figure A.10.1.3A: Center notch of the wing.....	35
Figure A.10.1.3B: Hole for the notch to center the wing.....	36
Figure A.10.2.1: Construction of the wing showing the balsa spars and foam ailerons.....	36
Figure A.10.2.2: Servo mount for the aileron.....	36
Figure A.10.3.1: Top view of final horizontal and vertical tail design.....	37
Figure A.10.3.2: Side view of final horizontal and vertical tail design.....	37
Figure A.10.4.1: Top view of motor mount extension.....	38
Figure A.10.4.2: Motor mount extensions without the 3D printed brace.....	38
Figure A.10.4.3: Aluminum spacers.....	38
Figure A.10.5.1: Isometric view showing the payload weight slides.....	38
Figure A.10.5.2: Fabricated weight payload.....	39
Figure A.10.6.1: CAD of payload drop-off mechanism.....	39
Figure A.10.6.2: Bottom view showing cargo bay doors opened and pusher.....	39
Figure A.10.7.1: Main landing gear.....	40
Figure A.10.7.2: Tail landing gear.....	40
Figure A.10.7.3: Tail landing gear side view.....	40
Figure A.10.8.1: Support Housing.....	41
Figure A.10.8.2: Rear control configuration.....	42
B.4.1: Gross Weight Equation:.....	42
B.4.2: Scoring Function Equation.....	42
B.5.1: Taildragger Landing Gear Equation.....	42
B.6.1: Total Drag Coefficient Equation.....	43
B.6.2: Drag Buildup — form and interference drag Equation.....	43
B.6.3: Reynolds Number Equation.....	43
B.6.4: 3-D Maximum Lift Coefficient Equation.....	43
B.7.1-4: Aircraft Takeoff Distance Equations.....	43
B.7.5-6: Climb and Maneuvering Thrust to Weight Equations.....	43

B.8.2: Elevon Area Equation.....	44
B.9.1: Horizontal and Vertical Tail Planform Area Equation.....	44
B.9.2: Center of Gravity Location Equation.....	44
B.9.3: Horizontal Tail Lift Curve slope Equation.....	44
B.9.4: Neutral Point Location formula.....	44
B.9.5: Static Margin Equation.....	44
Table C.4.1: Scoring Function's fixed parameter values.....	45
Table C.4.2: Scoring Function's Parameter Assumptions and Values.....	45
Table C.4.3: Assumptions on initial gross weight and wing area based on student-built aircrafts (MAE 155B).....	45
Table C.5.1: List of the fixed components and available components.....	46
Table C.5.2: List of the available parts and materials.....	46
Table C.5.3: List of the other available parts and materials.....	47
Table C.5.4: List of the propeller choices.....	47
Table C.6.1: Drag buildup for the 3D drag aerodynamic analysis.....	47
Table C.8.1: Specifications of the required brushless motor.....	48
Table C.8.2: Specifications of the required battery.....	48
Table C.8.3: List of the fixed components and available components.....	49
Table C.8.4: List of the propeller size choices and corresponding RPMs.....	49
Table C.9.1: List of individual component's mass and center of gravity location from fuselage structure nose along X axis.....	50
Table C.9.2: Aerodynamic parameters used to calculate Neutral point.....	50
Table C.9.3: List of various off shelf propellers for Cobra C2217 motor at set 11.1 input voltage. [5]...	
51	

Nomenclature

x	Aircraft design	W_g	Gross weight
$W_p(x)$	Payload 1 weight (high weight)	W_p	Payload weight
$V_p(x)$	Package 2 volume (high volume)	W_e	Empty weight
$E_f(x)$	Energy consumption	W_s	Energy-storage weight (batteries)
$W_g(x)$	Gross weight	W_f	Fuel weight
$T_f(x)$	Flight time	W_b	Battery weight
r_{wp}	Revenue per unit weight	V_p	Payload volume
r_{vp}	Revenue per unit volume	R	Range
c_e	Cost per unit energy	η_b	Conversion efficiency (battery to thrust power)
c_c	Cost per flight	e_b	Battery specific energy (energy per unit mass)
c_{Wg}	Cost per unit gross weight	g	Acceleration due to gravity
c_f	Fixed operating cost	$\frac{L}{D}$	Lift-to-drag ratio in cruise
$t_{;}$	Total aircraft-lift flight time	D	Propeller diameter
$C_{l,max}$	2D maximum lift coefficient	R	Propeller radius
C_{Lmax}	3D max $c_L \doteq 0.9C_{l,max} \cos\Lambda$	c	Chord (radial distribution)
C_d	2D drag coefficient	β	Pitch or twist (radial distribution)
C_D	3D drag coefficient	ω	Angular speed (rad/s)
$C_{D,0}$	Parasite drag coefficient at zero lift	n	Rotational speed (rev/s)
S	Wing area	V_∞	Inflow velocity

AR	Aspect ratio	C_T	Thrust coefficient := $\frac{T}{\rho n^2 D^4}$
Λ	Wing sweep (quarter-chord line)	C_Q	Torque coefficient := $\frac{Q}{\rho n^2 D^5}$
λ	Taper ratio := $\frac{c_{tip}}{c_{root}}$	C_P	Power coefficient := $\frac{P}{\rho n^3 D^5}$
t/c	Thickness-to-chord ratio	J	Advance ratio := $\frac{V}{nD}$
γ	Dihedral	η	Efficiency := $\frac{TV_\infty}{Q\omega}$
Re	Reynold's number	S	Disk area := πR^2
p	Air Pressure	T/S	Disk loading
T	Air Temperature	FOM	Figure of merit := $\frac{T}{P} \sqrt{\frac{T}{2\pi R^2 \rho}}$
ρ	Air density	$d_{forward}$	horizontal distance from the CG's vertical line to the main wheels
q	Dynamic pressure	h_{CG}	height of the CG above the ground
e	Oswald efficiency factor	θ	Target angle
μ	Dynamic viscosity		
$C_{d,min}$	2D minimum drag coefficient		
$C_{l,min}$	2D minimum lift coefficient		
α_0	Angle-of-attack at $C_l = 0$		

1. Executive Summary

The objective of this project was to design a remote-controlled (RC) delivery aircraft capable of simulating multi-package missions while maximising profit per flight. The aircraft was required to carry two distinct packages: a weight-based payload (≥ 0.5 lb) and a volume-based payload (≥ 500 cm 3). Using the scoring function in Appendix B.4.2, mission analysis showed that prioritizing the weight-based payload yielded higher returns, guiding the design toward minimal volume payload integration.

Initial sizing targeted a cruise speed of ~ 20 m/s, wing loading of ~ 2 lb/ft 2 , and a thrust-to-weight ratio of ~ 0.8 , resulting in a projected gross weight of ~ 2 kg and a wing area of ~ 0.27 m 2 . A high-wing configuration with a 3° dihedral improved roll stability, utilizing a lightweight balsa rib-and-spar wing and a semi-monocoque plywood fuselage with cutout for weight reduction. A taildragger gear layout provided favorable takeoff performance, servo-actuated hatch doors were implemented for in-flight volume payload deployment.

Final sizing closely matched initial estimates, with a measured gross weight of 2.1 kg and confirmed thrust-to-weight ratio of 0.83. Flight testing validated the aerodynamic performance, but revealed a CG location beyond the target 25-33% chord range, leading to tail-heavy instability. To correct this, post-flight adjustments included replacing foam empennage components with lighter balsa semi-monocoque structures and repositioning the propulsion system forward approximately 55mm. These changes eliminated the need for nose ballast and brought the CG within acceptable bounds. Additional reinforcements addressed motor mount reliability and landing gear stress.

The final aircraft configuration proved structurally sound, stable, and mission-effective, fulfilling all delivery and scoring objectives while demonstrating flight-worthy performance under test conditions.

Table 1.1: Aircraft Requirements and Specifications supervised in MAE 155B Course.

MAIN AIRCRAFT SPECIFICATIONS		FLIGHT REQUIREMENTS
Empty Weight	3.08 [lb]	1 The payload packages must consist of lead weights [P1] and an empty cube cardboard box [P2].
Gross Weight	4.58 [lb]	2 The payload weight must be at least 0.5 lbs [P1] and volume at least 500 cm³ [P2].
Payload Weight	1.50 [lb]	3 Mission Bay Park atmospheric condition parameters: pressure, p , of 101.28 kPa , temperature, T , of 286 K , density, ρ , of 1.23 kg/m³ , and dynamic viscosity, μ , of 1.80×10^{-5} Pa·s
Payload Hold Volume	42.875 in 3	
Empty Weight Fraction	0.67	4 Flight Area Range minimum of 600 m
Wingspan	3.77 [ft]	
Aspect Ratio	6.75	
Wing Loading	2.09 [lb/ft 2]	
Thrust-to-Weight	0.5	
Cruise Speed	65.62 [ft/s]	

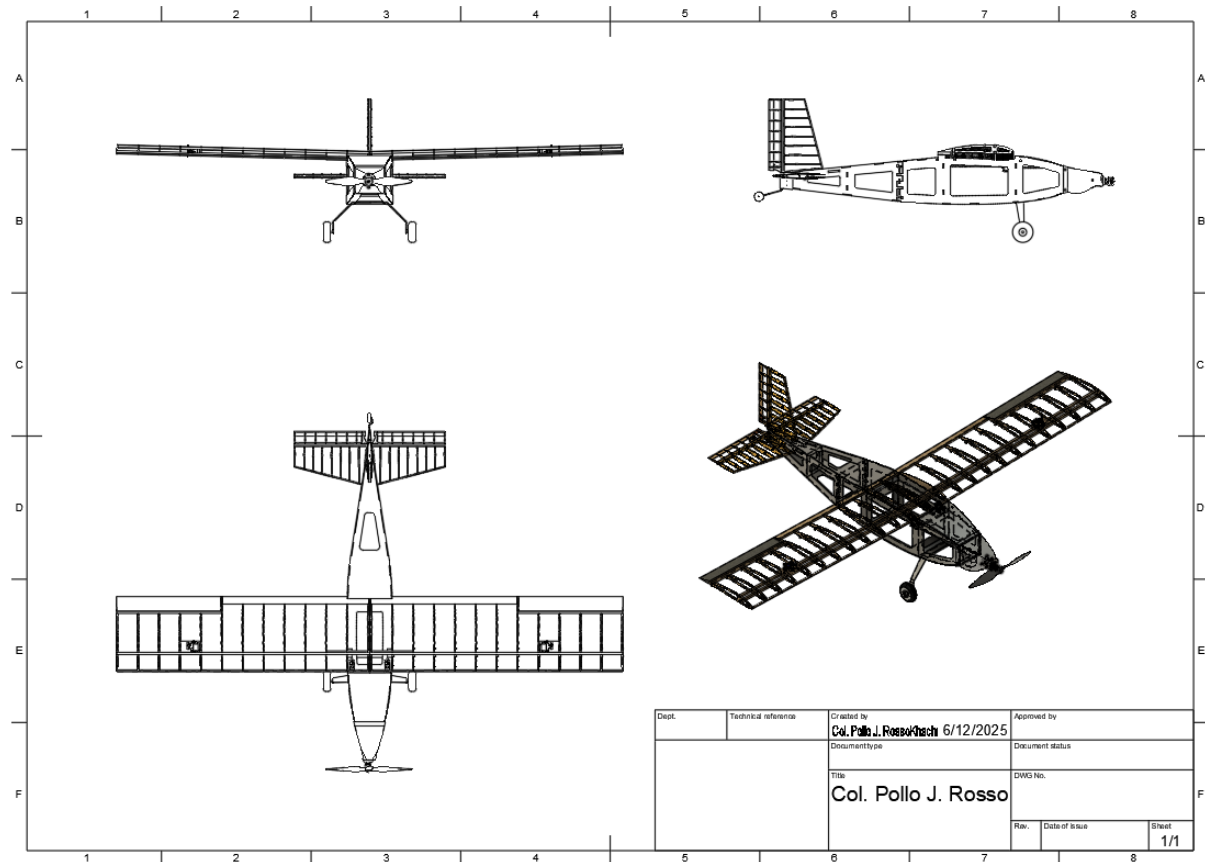


Figure 1.1: Isometric and 3-view of the aircraft.

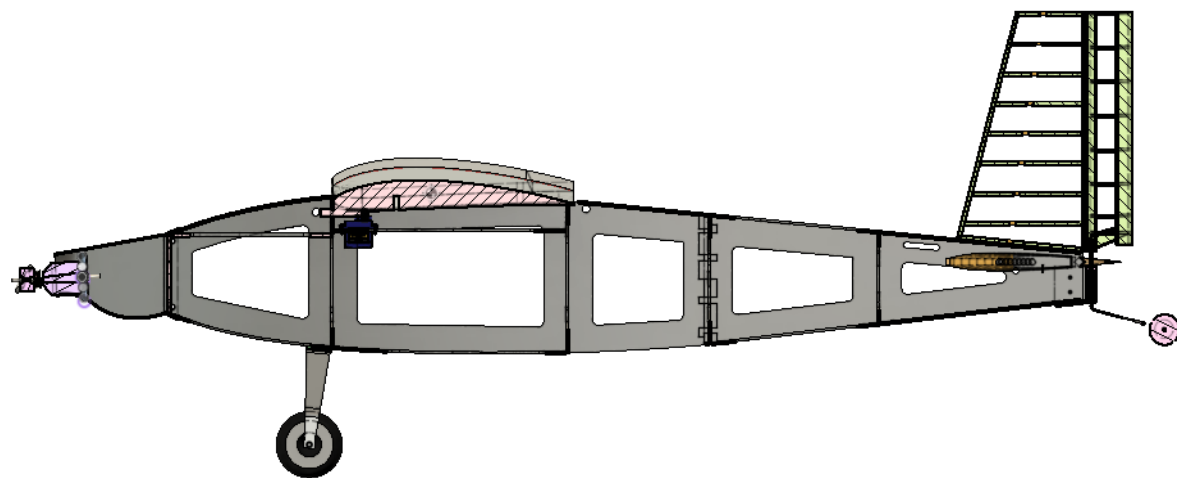


Figure 1.2: Cross sectional view of the aircraft.

2. Introduction

In our post-pandemic world, e-commerce giants like Amazon, Doordash, and Walmart are rapidly expanding their reach to provide fast, reliable, and sustainable delivery services. Unmanned aerial systems, such as RC planes can fill the niche of fast delivery with minimal environmental impact. Such capability is especially valuable during certain situations such as delivery of medical equipment in remote locations and rapid deployment of critical components. The RC plane proposed is designed to accommodate two distinct payload configurations: high weight with low volume [P1], and high volume with low weight [P2].

CATEGORY	ASPECT
Financial	<ul style="list-style-type: none"> \$720 total budget allotted
Mission & Maintainability	<ul style="list-style-type: none"> Our goal is to carry two packages, a high-weight and a high-volume; only dropping off the latter
Environmental Factors	<ul style="list-style-type: none"> Zero emissions and low noise from a battery-powered propeller
Structures & Weights	<ul style="list-style-type: none"> Structural integrity is maintained by utilizing low-weight balsa wood frames and carbon fiber spars

Table 2.2: Measures of Merit

3. Concept of Operations

3.1 Requirements and Constraints

REQUIREMENTS	CONSTRAINTS
Airframe: wing, fuselage, horizontal tail, vertical tail, landing gear	Motor: Cobra C-2217/16 Brushless, Kv=1180
Propulsion system: propeller, motor, speed controller, battery, (battery charger)	Speed controller: Flite Test 40 Amp ESC
Radio control: receiver, (transmitter, transmitter battery)	Battery: Tattu 11.1V 1800mAh 3S 45C LiPo
Actuation: control surfaces, servos, servo push rods, control horns, servo extensions	Receiver: FrSky Taranis Receiver X8R 8 Channel 2.4 GHz
Easily Accessible: easily removable watt meter and battery	ESC: Powerwerx Watt Meter-Bare, DC Inline Power Analyzer, 45A Continuous

Table 3.1: Targets and Constraints for a radio-powered aircraft

3.2 Operations and Mission Profile

All aircrafts are expected to perform a ground roll test for the aircraft's yaw control from the contact between the flight area's dirt field and the landing gear. This test allows the pilots to familiarize themselves in landing the aircraft. There are two primary flight missions to be

performed. In *Table 3.2*, a successful empty payload flight allows the team to perform the payload flight. The payload flight demands to carry both payloads, the weight-based [P1] and volume-based payload [P2], and to eject only the volume-based payload midair at a designated point. Although the aircraft's glide ability is imperative, it is expected that it can survive multiple crashes and be repaired easily.

MISSION #	PAYOUT	DETAILS
1	Empty	Perform a successful flight without payload to participate in the competition, required to perform the next mission
2	Weight-Based [P1] & Volume-Based [P2]	Carry a package consisting of lead weights, with a minimum weight of 0.5 lbs and eject an empty cubical box mid-air, with a minimum volume of 500 cm ³ ;

Table 3.2: The two missions of the aircraft and corresponding descriptions.

4. Sizing Analysis

4.1 Scoring Function

To evaluate the effectiveness and overall performance of our aircraft design, we were given a scoring function that incorporates payload delivery capabilities, energy efficiency, flight duration, and other operational cost parameters. Our goal was to maximize our performance by finding the highest score we can get using the function *Appendix B.4.2*. The fixed operational cost parameters are provided in *Appendix C.4.1*. Since the values are fixed and constant, the scoring function can be simplified and weighed by the aircraft overall weight $Wg(x)$, payload weight $Wp(x)$, payload volume $Vp(x)$, battery energy consumption $Ef(x)$ and the overall flight time $Tf(x)$. Changing the values of these parameters yield both gains and trade-offs. The simplified scoring function will guide us in designing our aircraft.

Using the scoring framework, we simplified the aircraft's battery consumption $Ef(x)$ as it depends on the thrust required to maintain cruise and power input, which can further be reduced to a function that depends on our assumed lift-to-drag ratio L/D and cruise speed. Our energy source, an 11.1V 1.8Ah battery, was estimated to provide 453,070 J/kg and was assumed to have an efficiency of 85%. The other assumptions are given in *Appendix C.4.2*. We are able to conclude that the cost of increasing the energy consumption is negligible through $Ef(x)$'s low quantitative value. Like the energy consumption, the overall flight time heavily depends on cruise speed in which we don't have liberty to control as the aircraft is powered by one motor. We acknowledge that our scoring function will ignore the effects of $Ef(x)$ and $Tf(x)$.

In the end, our team decided that one of the goals of the scoring function analysis was to find the right payload volume to design our fuselage around. With this, we compromised on increasing the payload volume from minimum up to a volume of 64 in³. We will be designing a

fuselage that can accommodate this cubic volume. We concluded that the scoring function will only be a stepping stone to start our aircraft design. Another goal was to compromise on a starting payload weight, a minor constraint for us, such that we can increase it depending on the future aircraft performance results. We are only physically capable of increasing the payload weight with a J gain [\\$] of 7.5 \\$ per unit weight *Table 4.1*, mainly because the payload weight will strategically be placed around the center of gravity (CG). Steadily increasing its value will have more benefits than increasing the payload volume. For now, our payload weight is compromised to be 1.5 lb and will be subjected for changes.

	ASSUMPTION	VALUE
J [\\$] gained per unit payload weight, W_p	fixed V_p of 500 cm ³	7.50 \\$/lb
J [\\$] gained per unit payload volume, V_p	fixed W_p of 0.5 lb	2.25 \\$/cm ³

Table 4.1: The J gain [\\$] per unit increase of a payload parameter, while keeping the other fixed

5. Configuration and Concept Design

The aircraft development heavily focuses on meeting the operational requirements, which corresponds to the minimum payload weight and volume. The scoring function analysis has provided the additional weight we can add into the aircraft, specifically how much payload weight until the drawbacks outweigh the score increase. The aforementioned analysis also revealed the limited volume range of the cubical box payload. The fuselage design will prioritize maintaining structural integrity while also accommodating an assumed 64 in³ cardboard box and other components. The wing will be designed based on an airfoil that maximizes lift best among selected airfoils. Its dimensions are calibrated to provide substantial lift for the aircraft, and its skeletal structure will be optimized for weight and overall wing structural integrity. A taildragger landing gear configuration was decided in order to improve the aircraft's takeoff and landing performance due to the additional angle-of-attack for the wing. Another reason is to minimize the possible interference of the package drop-off mechanism with the landing gears. Lastly, a cargo door mechanism will be adopted to drop the package mid-air. It will undergo several adjustments to incorporate reliability during unloading, straightforwardness, and practicality in terms of maintenance. Together, these elements will form a cohesive design that balances performance, functionality, and manufacturability. Component details are in *Appendix C.5*.

5.1 Wing Design

In terms of wing structure construction, we adopted a rib-and-spar configuration made with balsa wood. Balsa offers an excellent balance between strength and weight, which allows us to keep the structure lightweight and still obtain sufficient stiffness to handle aerodynamic wing loads. The use of balsa wood ribs allows an easier manufacturing process and modification when it comes to design refinements. The aforementioned refinement pertains to keeping the aircraft

lightweight and structurally durable. Compared to using foam, this approach has room to improve the wing's overall performance and also emphasizes adaptability to future revisions.

A high-wing configuration was selected with a positive dihedral angle of 3° to enhance flight stability, particularly along the roll axis. This allows an improvement to the aircraft's ability to self-correct after a disturbance, events when the aircraft banks due to a gust or a maneuver. The dihedral effect produces a restoring moment that aids the aircraft to return to level flight without excessive pilot or autopilot input. This configuration is especially useful for maintaining consistent and stable flight during package transport missions.

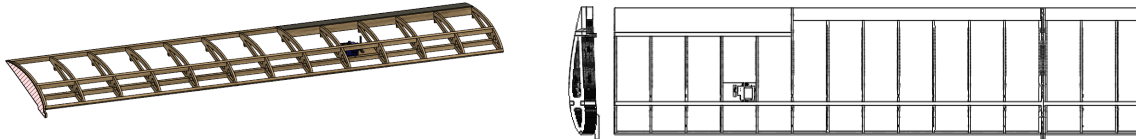


Figure 5.1: The skeletal wing structure design with wooden rib and spars, along with aileron.

5.2 Fuselage Structure

A simple box-shaped design built from lightweight plywood was adopted for the fuselage. As mentioned in previous configuration justifications, manufacturing should be easy to execute while also keeping structural integrity in mind. An initial box form fuselage naturally provides the best room to house the packages and critical onboard components without complicated manufacturing. The use of plywood makes the fuselage rigid and durable and allows it to handle flight loads and landing forces.

Further attempts to reduce weight were executed by making material cutouts in non-critical areas, basically trimming down some structural dimensions and also supporting areas where stresses are expected to be the highest. From the initial box design, curves were added to the fuselage structure to keep the incoming airflow continuous, effectively improving the aircraft's aerodynamic performance. Quantitatively, we are able to reduce weight by 200 g from material cutouts. Detailed analysis will be made to verify the overall structural integrity.

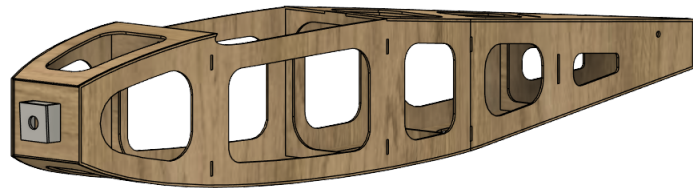


Figure 5.2: The CAD skeletal structure of the aircraft fuselage.

5.3 Landing Gear Choice

A taildragger configuration was selected for the landing gear design to improve control during the aircraft's missions. This configuration naturally offers a higher angle-of-attack for the wing and tails during takeoffs, providing better lift and significantly reduces the takeoff distance. It also provides greater ground clearance, which is imperative as the operations are done on rough and uneven runways. Better clearance helps protect the propeller from hitting the ground. The fuselage will be vertically displaced better, reducing the possible damage of debris to the drop-off mechanism. Overall, this configuration supports aerodynamic performance and control during ground roll tests.

The aircraft taildragger landing gear will be positioned strategically to ensure ground roll stability, an overall safer takeoff performance. One common design guideline is to place the main wheels where the level ground attitude, the line from the center-of-gravity (CG) to the main wheel's contact point, forms an estimated angle of about 12° to 15° forward from vertical. This geometry prevents nose-over during brakes or rough landings, while it allows the wing and tail to provide lift easily during takeoff. It helps to balance the weight distribution, with about 15-20% weight burden to the tailwheel that is ideal for stable and efficient ground handling. *Equation 5.1* will be used to find the needed landing gear dimensions, keeping the assumed angle in mind.

5.4 Payload Drop-off Mechanism

The payload flight mission mandates the drop-off of the 64 in³ volume-based payload [P2] during flight. The payload drop-off requires a reliable and secure door mechanism design, guaranteeing that the payload is ejected without becoming stuck inside its compartment. In addition, the doors must close properly after drop-off to minimize the drag caused by a non-continuous airflow below the fuselage. The initial concept development has a two-door design with two different mechanisms. The gear-driven mechanism is proposed to control the opening and closing of the doors. Another mechanism employs lever arms to open the doors mechanically during payload release. A spring-loaded system will be added to safely eject the payload out of the compartment. Further physical testing will be required to determine the most effective, fastest and safest package release, keeping the aerodynamic penalties to a minimum.



Figure 5.3: The two proposed mechanisms for two-door opening and closing, gear-driven (left) and lever (right)

6. Aerodynamics

6.1 Assumptions

To properly define the aerodynamic characteristics of our aircraft, we first analyzed the expected flight atmospheric conditions. The main wing dimensions are set in *Table 6.1*. The standard atmospheric conditions of Mission Bay Park, the flight area, were provided in *Table 1.1*. Assuming a cruise speed of 25 m/s and a mean chord length of 0.2 meters, we estimated a Reynolds number (Re) of approximately 340,000 *Appendix B.6.3*. This value reflects the flow regime around the airfoil and helps determine aerodynamic performance. Given that airfoil performance data is more readily available at standard Reynolds numbers, we selected airfoils characterized at $Re = 500,000$ to ensure a conservative and reliable match for our design. Using data from the XFOIL database, we extracted the relevant lift, drag, and parasite drag coefficients for our calculations and performance modeling.

PARAMETER	VALUE	PARAMETER	VALUE
Planform Area (m ²)	0.27	Aspect Ratio	6.75
Wing Span (m)	1.397	Taper Ratio	1
Chord (m)	0.2	Sweep	0

Table 6.1: Main wing dimensions

6.2 Airfoil Selection

To determine the optimal airfoil for our wing design, we conducted a 2D aerodynamic analysis using XFOIL at a Reynolds number of 500,000, based on our expected flight conditions of cruise speed of 25 m/s and chord length of 0.2 m. We evaluated five widely used airfoils—NACA 4412, 4415, 2412, 0012, and Clark-Y—focusing on lift coefficient (C_l) and drag coefficient (C_d) across a range of angles of attack. As shown in the performance plots, NACA 4412 demonstrated the most favorable characteristics, achieving a maximum C_l of 1.362 at a stall angle of 13.25°, which is the greatest lift coefficient among competitors. Its minimum drag coefficient, C_d , is 0.0363, however, most of the airfoils have their drag coefficient around that. Our airfoil selection was decided to be the airfoil that provides the best lift among the other candidates as all of the airfoils' drags are quite identical.

These values indicate strong lift performance, efficient cruise behavior, and smooth stall characteristics. Based on this comprehensive comparison, we selected NACA 4412 as our primary wing airfoil for its superior low-speed aerodynamic efficiency and reliability.

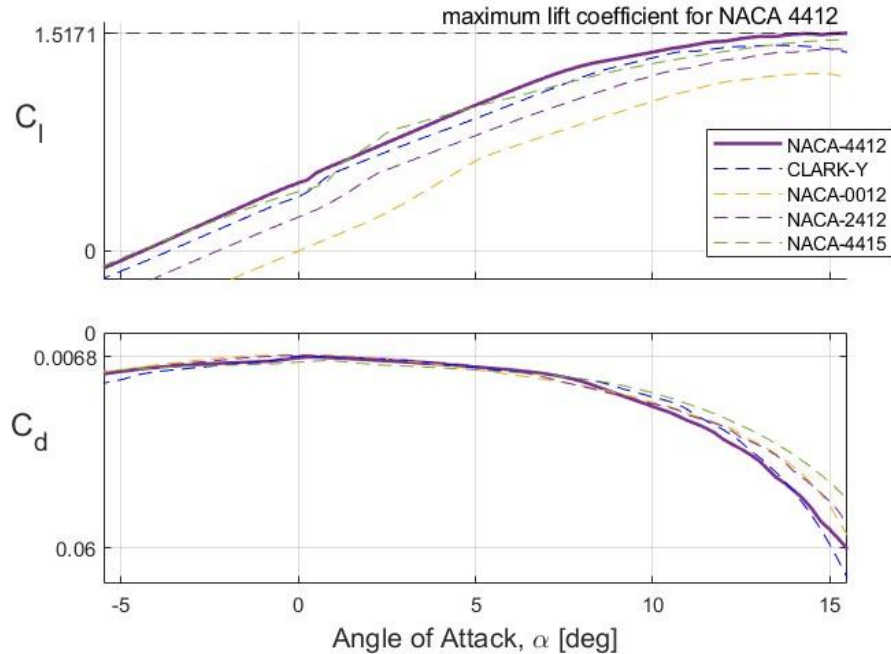


Figure 6.1: Selected Airfoils 2-D Aerodynamic Analysis at $Re = 500,000$ and cruise speed of 25 m/s. Data imported from XFOIL. Lift Coefficient (top) and Drag Coefficient (bottom) vs Angle of Attack. Stall Angle of Attack at 13.25°

PARAMETER	VALUE	PARAMETER	VALUE
CL_{max}	1.36222	AOA stall	13.25°
CD_{min}	0.0363	S_{wet}/S_{ref}	2.0480
$(L/D)_{max}$	35.838	K''	0.01344
Cl_{min}	-0.8699	a_0	-4.5°

Table 6.2: Major Aerodynamic Parameters of selected airfoil, NACA 4412.

6.3 Drag Buildup

To estimate the total drag of the aircraft, we used the drag build-up method based on Raymer's approach, incorporating skin friction coefficients (C_f), form factors (FF), interference factors (Q), and wetted area ratios (S_{wet}/S_{ref}) for each major component. Starting from 2D XFOIL data, we derived $K'' = 0.01344$ and calculated 3D lift and drag coefficients for a more realistic representation *Appendix A.6.1*.

The wing section had a C_f of 0.0023, FF of 1.0521, and S_{wet}/S_{ref} of 2.048, resulting in a CD_0 of 0.0054. The fuselage contributed 0.0063, while the motor and landing gear added 0.019 and 0.0057, respectively. Tail drag contributions were assumed small and are pending

refinement. The total parasite drag coefficient (CD_0) was estimated at 0.0363, which matches the minimum value on the plotted 3D drag curve. This curve includes the aerodynamic effects of the full aircraft and a more detailed drag buildup for each aircraft part is in *Appendix C.6.1*.

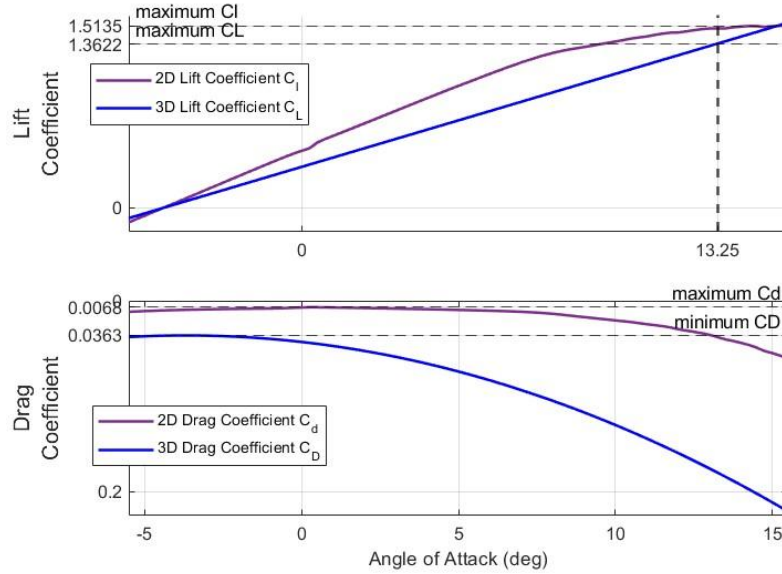


Figure 6.2: 2-D and 3-D comparison. Lift coefficient with CL_{\max} at 13.25° stall angle of attack (top); Drag coefficient vs angle of attack, 3-D includes the drag build-up for wing, fuselage, tails, propeller and landing gear. (bottom)

7. Performance

7.1 Takeoff

In order to calculate the initial takeoff distance (SG) and performance of the aircraft equations 7.1-7.4 was implemented in a MATLAB code with the estimated gross weight, wing loading, and wing design parameters from the initial sizing as illustrated in *Figure A.7.1*. Additionally due to rough runway conditions at Mission Bay park the rolling friction coefficient was assumed to be 0.03. This resulted in a takeoff distance of around 12.26 meters with a corresponding stall speed of 9.314 m/s. This gives a rather quick takeoff performance on par with similar RC aircraft in a sport category which would further be improved due to the plane's tail dragger configuration. Furthermore, due to the large runway distance (~80 m) at mission bay as shown in *Figure A.7.2* this plane design provides ample room in case of emergencies or issues at takeoff. While these are the expected values for the weighted flight during takeoff for the maiden flight was around 6 meters at a gross weight closer to 1.7 kg which demonstrates how well our plane can perform even in windy conditions as seen in the maiden flight.

7.2 Cruise

Since the goal of this design was to minimize the flight time as much as possible the calculation of thrust versus cruise velocity was utilized to find the total range of values, and the nominal cruise speed based on the chosen propeller/motor combination. In order to get a more accurate representation of this plot the 3D aerodynamic coefficients and the estimated max gross weight of 2 kg was used. This assumed steady level flight as such lift was set to gross weight and thrust was set to equal drag.

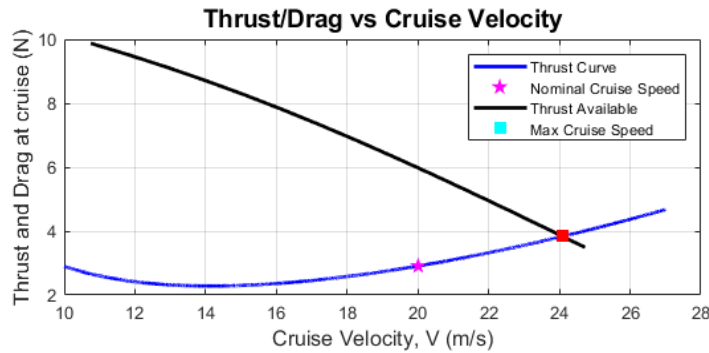


Figure 7.1: Thrust required for steady level flight given different cruise velocities.

As illustrated in *Figure 7.1* the thrust required at nominal cruise speed is around 3 newtons and the max cruise speed given propellers available thrust at max power calculated at 3.83 N gives a max cruise speed of 24 m/s.

7.3 Maneuvering and Climb

With the designed wing loading, 3D aerodynamic coefficients, 2 kg gross weight, and desired 0.5 thrust to weight ratio it was found that our maximum load factor during maneuvering is that of 4 and the maximum climb angle was that of 15° using *Appendix B.7.5-6* as highlighted in *Figure 7.2*.

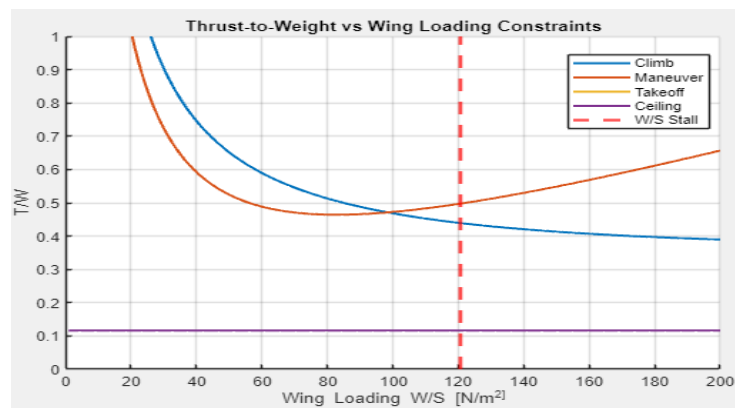


Figure 7.2: T/W vs Wing loading at set performance and aerodynamic design parameters.

These two values ensure a very agile and quick performance necessary for the proposed mission segments and target goal of minimizing flight time. Furthermore during the maiden flight it was found that the plane was very capable of quick maneuvering and even able to do a loop!

8. Propulsion

8.1 Propulsion System Design

The propulsion system of the aircraft consists of a Cobra C-2217/16 brushless motor with a given input voltage of 11.1V. We calculated a maximum motor speed to be approximately 13098 RPM. Considering an operating range of 50-80% of this maximum, the usable RPM range becomes roughly 6500 to 10500 RPM. As stated in the performance section, we have determined that the thrust needed to maintain our 20 m/s cruise speed is 3N. With these constraints a propeller analysis was required to determine the correct sizing for our aircraft. Within the target RPM range, we compared various suitable propellers *Appendix C.9.3*. The APC 8x6-E propeller demonstrated the highest efficiency (η) versus advance ratio (J) in Figure 1, with the APC 9x6-E closely behind. Although the 8x6-E showed superior efficiency, power coefficient (C_p), torque coefficient (C_q), and thrust coefficient (C_t) across *Appendix A.8.1-4*. However, further evaluation, using *Table 8.1*, revealed a critical performance shortfall: the APC 8x6-E fails to meet the required 3 N of thrust at cruise. This level of thrust is only achieved above 9000 RPM, which pushes the motor to operate near the upper limit of the defined range – exceeding our efficiency and reliability constraints. In contrast, The APC 9x6-E delivers a more favorable thrust profile at cruise conditions. At 9000 RPM, it produces approximately 3.75 N of thrust, compared to only 2.66 N from the APC 8x6-E. Given its ability to meet thrust requirements within the acceptable RPM range and its performance at the cruise advance ratio, the APC 9x6-E was selected as the optimal propeller for our aircraft.

Propeller	η_p	Thrust [N]	Torque [Nm]	Power [W]	J	n [RPM]
9x6E	0.724	3.75	.112	105.29	0.583	9000
8x6E	0.736	2.66	0.077	72.20	0.655	9000

Table 8.1: Propulsion Key Parameters comparison between 9x6E and 8x6E.

9. Weights and Balances

9.1 Weight Breakdown

Whilst initial sizing estimates with the desired gross weight had changed the distribution of mass in the final iteration of the plane it was still on par with previous calculations with the measured mass of the final iteration of the plane being illustrated in pie chart on the left of figure 9.1. From this it was calculated that about $\frac{1}{3}$ of the total gross weight came solely from payload 1 whilst both the fuselage and wing had about a $\frac{1}{6}$ of the gross weight each. As a result the estimated empty weight fraction was found to be 0.67. In terms of the structural weight of the plane highlighted by the pie chart to the right of figure 9.1 the plane is $\frac{2}{3}$ made of wood followed

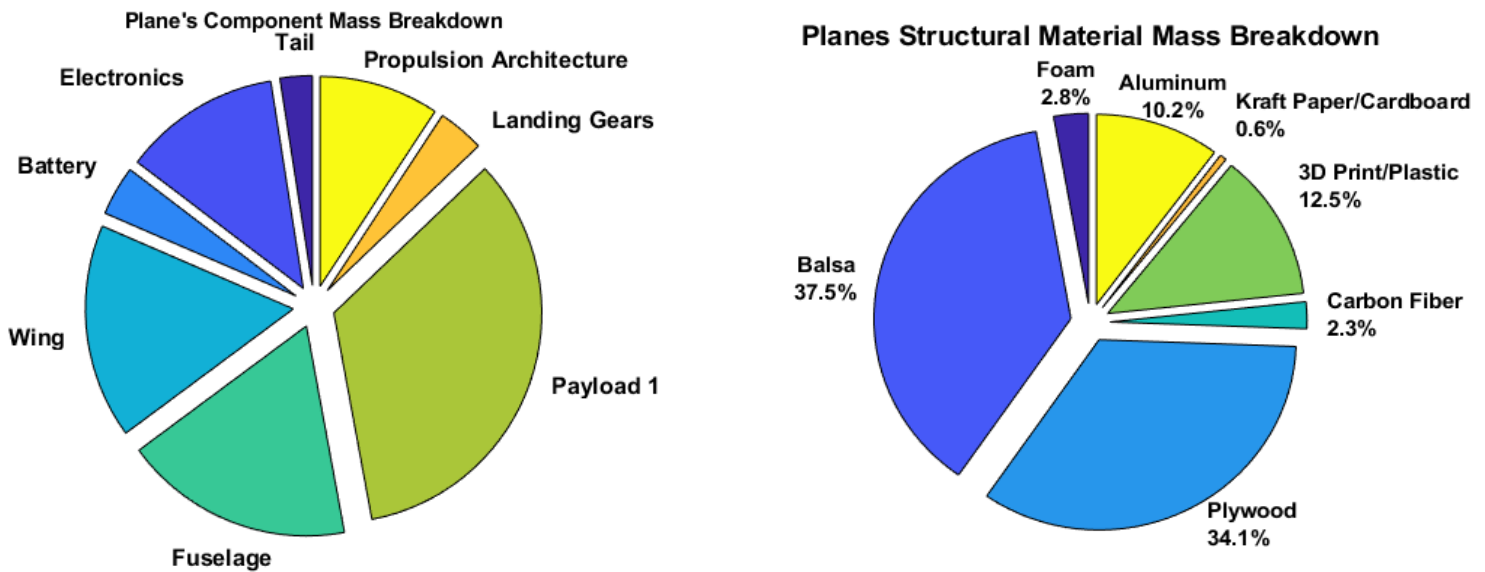


Figure 9.1: Breakdown of Aircraft Weight and Material Composition

by 3D printed plastic, and aluminum as the 3 most used materials in the plane's structural design which highlights the overall ease of manufacturing and cheap cost that this design maintains.

9.2 Tail Sizing and Configuration

Since the goal of the plane is to achieve a quick flight time with agile maneuvering the tail sizing needed to reflect the adequate control and stability necessary. As such the empennage was designed with a traditional T-tail configuration. Additionally the vertical tail used a volume coefficient that is based off of reference craft and the homebuilt value illustrated in *Figure A.9.2* of the appendix which corresponded to a C_{VT} and C_{HT} of about 0.035 and 0.4 respectively. To

further minimize drag and structural weight an aspect ratio of 3.5 and 1.26 for horizontal and vertical tail was chosen with the moment arm distance (i.e. distance from wing quarter-chord to tail quarter-chord) for both tails set to 0.42 m. With the volume coefficients, moment arms, wing area, and wing span the tail area was calculated using *Appendix B.9.1* [1] producing the results in *Table 9.1*. While the horizontal stabilizer is rectangular the vertical tail was tapered at a 0.65 ratio to reduce structural weight whilst maintaining adequate rudder control. To achieve great stability, agility, and sufficient tail authority both vertical and horizontal tails utilized a NACA 0012 airfoil due its ability to satisfy the aforementioned characteristics in addition to its proven reliability and symmetric shape for aerobatic maneuvers.

PLANFORM AREA	VALUE
Vertical Stabilizer (S_{VT})	0.0304 m ²
Horizontal Stabilizer (S_{HT})	0.0514 m ²

Table 9.1: Tail Sizing Dimensions

9.3 Control Surfaces

Using reference RC aircraft of the aerobatic class and Raymer textbook the elevator, rudder, and ailerons were sized as highlighted in Table 9.2. Additionally to achieve adequate control for the plane the control surfaces were mechanically designed with the deflection angles found in the aforementioned table.

Parameter	Elevator	Rudder	Ailerons
% of Chord	33%	32%	20%
% of Span	100%	100%	40%
Deflection [deg]	± 30	± 20	± 15

Table 9.2: Control Surface Sizing

9.4 Static Stability

To achieve stability in flight the initial goal was to place the plane's center of gravity at the quarter chord in all 3 flight configurations (empty, takeoff, dropoff). This led to the placement of individual masses/components detailed in *Table 9.1* along for which was inputted to *Appendix B.9.3* to find the overall CG location with the reference point being the nose of the fuselage structure. As such this resulted in the CG locations found in *Table 9.2* in which all three configurations are slightly forward of the wing quarter-chord location providing ample self correcting stability during flight in case of strong wind gusts which is typical in coastal regions like Mission Bay Park which was indeed seen in the maiden flight. In addition to CG location the neutral point and static margin were calculated using inputs from *Appendix C.9.2* into *Appendix B.9.3-5* resulting in a static margin range from 16-18% from the mean aerodynamic chord. With

this range of static margin the plane is set to be more than adequately stable ensuring safe and maneuverable flights in most conditions particularly coastal wind gusts.

Stability Parameters Results	Percentage (%) from MAC
Center of Gravity (Empty Flight)	25.73
Center of Gravity (w/ Payloads 1 & 2)	25.05
Center of Gravity (w/ Payloads 1)	24.97
Neutral Point	41.27
Static Margin(Empty Flight)	15.52
Static Margin(w/ Payloads 1 & 2)	16.22
Static Margin(w/ Payloads 1)	16.32

Table 9.2: Aerodynamic stability results

10. Completed Structural Framework

10.1 Fuselage

To achieve an aerodynamic shape and accomplish the requirement for a taildragger configuration, the semi-monocoque fuselage was by combining a rectangular box and a rectangular prism, with the latter being the place for the rear landing gear. The fuselage can be divided into five parts, starting with a 3mm thick firewall in front. The plywood firewall had slots to attach to the fuselage and cutouts for the motors mounts. The next section, pictured in *Appendix 10.1.1*, was allotted as the compartment for electronics and the 3D printed reinforcement plates, glued to the fuselage with epoxy. The reinforcement plates not only strengthened the fuselage but also served as the place for attaching the front landing gear with screws. The reinforcements, both 3D printed and plywood, helped account for the aircraft's impact resistance and torque loads. The next section, pictured in *Appendix 10.1.2*, includes holes for two carbon fiber tubes and an airfoil cutout at the top for the main wing placement. This fuselage part includes the payload weight inside and the main wing at the top. The wing slides into a cutout in the fuselage, where it will be fixed to the fuselage using rubber bands around the carbon fiber tubes and over the wing. A cutout slot in the bulkhead, shown in *Appendix 10.1.3A* and *10.1.3B*, allows for widthwise centering of the wing on the fuselage with a protrusion in the center of the wing. The remaining fuselage parts were designed for the payload volume drop-off mechanism and the rear landing gear.

10.2 Wing

Our final design, displayed in *Appendix 10.2.1*, mirrors our initial design, in which we are still using balsa ribs, shear webs, and skin and overcoat by MonoKote. The semi-monocoque design has 12 ribs on each side and one at the center shared between the two sides that also acts as a connection point, mentioned in section 10.1, to the fuselage that is enforced by double 1/16 " plywood, with 3mm ribs at the wing tips for extra reinforcement. The main spars were from

dowel wood, which excels in its strength performance compared to balsa wood. The 3 degree dihedral configuration was achieved by mounting the dowel wood spars onto a plywood center section glued with superglue and wood glue. Each half of the wing contains integration of mounts for servos to control the ailerons with metal linkage rods, pictured in *Appendix 10.2.2*. The ailerons were attached to the wing with plastic hinges, glued with epoxy.

10.3 Horizontal and Vertical Tail

Using the established sizing from section 9.2 both the horizontal and vertical tail were initially design with a foam core which was laminated with 1/32" balsa sheets and covered with monokote but due excess weight caused by epoxy the final iteration of the tail design utilized a wing ribs with carbon fiber design. The horizontal stabilizer design included 7 ribs made of 3 mm balsa and balsa sub spars in the leading edge and control surface mount location to support main carbon fiber spar. The vertical stabilizer design similarly utilized 9 ribs and 3mm balsa sub spars of the same dimension in the leading edge and control mount location. Both stabilizers had an additional 5x4 mm carbon fiber tube located at respective MAC. Both tail structures were assembled with super glue, coated in a layer of monokote and attached to laser cut locations on the fuselage with 1:1 epoxy resin as seen in *Figure A.10.3.1-2* of the appendix. Both the elevator and rudder were attached via 2 nylon plastic hinges superglued into rear sub spars.

10.4 Nose and Propulsion System

From Section 10.2, the fuselage firewall consisted of cutouts for the motor mount attachment. The motor mounts were made with 2mm plywood that displaced the motors by 15mm forward from the firewall. The interlocking wooden panel design was reinforced with epoxy. A 3D printed shim was added to achieve a 2° to the right and 3° down angle for the motor, counteracting the corkscrew effect of the single propeller. The flight test made us learn that the aircraft's weight was unbalanced, specifically tail-heavy, and this led us to add aluminum spacers to displace the propulsion system further [7]. The nose cone and the spinner design was discontinued because of vibrations that happened during the flight test. The mount cover was redesigned to account for the propulsion system forward displacement, but kept its aerodynamic shape. The propulsion system cover can conveniently be slotted into the fuselage front and screwed to the fuselage with four screws. The aforementioned details are shown in *Appendix 10.4.1-3*.

10.5 Weight Payload Compartment

The weight payload mount is designed with the assumption that the weight payloads will be attached securely to the fuselage but accessible and removable after flight. The main design is a simple square interlocking wooden panel assembly with removable slides, the weights will be attached to each side of a slide. The slide is designed to be removable from the wing access without having to remove the mount. Each slide can accommodate up to eight half ounce weights per side, an overall maximum weight of 2 pounds for all four slides. This allows for some

flexibility in the payload weight such that we could potentially add more weight for a higher flight score once the aircraft performance is verified. Additionally, the whole mount is attached to the fuselage with velcro allowing for adjustment with respect to aircraft CG.

10.6 Volume Payload Delivery

The payload drop-off mechanism was finalized by integrating a blend of the initial two design proposals. The final design integrated a twin servo design, where each individual servo drives a transfer gear that rotates the four-bar linkage system. By utilizing a python script to develop the correct length linkages, the bay doors were allowed to open slightly more than 90° with respect to the fuselage bottom, effectively fully deploying the volume package [P2]. The payload was also adjusted from the initial 64 in³ to 42.875 in³ in order for it to fit within the fabricated curved fuselage. This volume decrease allows room for the rubberband assistance mechanism. The assistance mechanism serves two purposes. It holds the top of the payload steady and keeps it pressed against the bay doors in-flight. During package deployment, the tensioned bands act as springs to assist forcing the payload out of the aircraft. The consideration for this assistance mechanism is due to the potential air resistance at delivery nominal cruise speeds, in which the lightweight box may not be able to the airframe. The updated bay doors include guides that help hold the payload during transit, as well as provision for 90° return springs to help assist the bay doors close and remain in their position throughout the flight. The actual and conceptual design are in *Appendix 10.6.1* and *10.6.2*.

10.7 Landing Gears

The landing gears are the same as the stock parts provided but with slight modifications. The main landing gear is bent higher so that the aircraft will sit higher from the ground, while the rear landing gear is bent aggressively so that the tail sits even lower. The maximum lift-to-drag was almost achieved by having a takeoff angle-of-attack of 11 degrees. Additionally, the rear landing gear is attached to the aircraft with a 3D printed mount that aligns the pivot point of the rear landing gear with the rudder hinge; this allows control of both rudder and rear wheel with one servo. The images are shown in *Appendix 10.7.1-3*.

10.8 Control System\

The control surfaces to the empennage were connected to servo motors through push-pull rods enclosed by plastic tubes. The servo travels ± 30 degrees which provides ample control for all maneuvers. The servos controlling the ailerons are located inside the wing, mainly utilizing the cutoffs in the ribs. A servo compartment was designed to keep the aileron servos in place. All of the electronics are primarily placed in front of the wing, inside the fuselage, where they are held intact using velcros. The other servo placements are illustrated in *Appendix 10.8.1-2*.

11. Post Maiden Flight Alterations

Following our maiden flight on June 6, 2025, there were several alterations made to the design to resolve issues we encountered. The primary issue we needed to address was the aircraft balance, with it being tail-heavy. The issue led the center-of-gravity (CG) of the aircraft to be at 60% of the chord, in contrast to the ideal 25-33% range. In order to achieve a successful flight on that day, we added 11 oz of ballast around the motor mount covers to shift the CG forward and to have a successful flight. The weights added and their corresponding distances from the CG helped us rebalance by displacing the propulsion system forward, potentially avoiding having to make changes on the flight competition day. Another solution we did was replacing the initial foam empennage with a balsa wood semi-monocoque design, effectively reducing tail weights. The other problem that revealed itself during the maiden flight was that the motor mount screws became completely unmounted from the fuselage while coming in for a landing due to vibrations from the motor. This resulted in a harder landing that put more force on the front landing gear than expected and minor damage to the fuselage. This was addressed by applying LOCTITE threadlocker to the motor mount screws on the new mount to prevent unscrewing, as well as 3d printing an additional brace to reinforce the frame where the landing gear connects. The landing gear itself was shifted forward 2 cm from the previous location to improve angle of attack and reduce risk of failure of damaged section of fuselage.

12. Conclusion

The Colonel was developed with the primary goal of maximizing payload-based profit while maintaining aerodynamic efficiency, structural simplicity, and operational reliability. Through a data-driven scoring function and careful trade-off analyses, our team prioritized carrying the heavier package while still accommodating a volume-based payload. The final configuration features a high-wing design with 3° dihedral for roll stability, a balsa rib-and-spar wing for lightweight strength, and a semi-monocoque plywood fuselage optimized for internal volume and manufacturability. A taildragger landing gear setup was selected to improve takeoff performance and increase ground clearance, especially for mid-flight payload drops. Aerodynamic efficiency was validated through 2D and 3D airfoil analyses, confirming the NACA 4412 as the optimal choice for low angle-of-attack. A drag build-up approach yielded a total parasite drag coefficient of 0.0363, guiding cruise and propulsion sizing. Propulsion analysis led to the selection of the APC 9x6-E propeller, capable of delivering the required thrust within efficient RPM ranges. With proven structural stability, balanced weight distribution, and strong aerodynamic performance, the Colonel is well-positioned to meet its dual-payload delivery mission successfully.

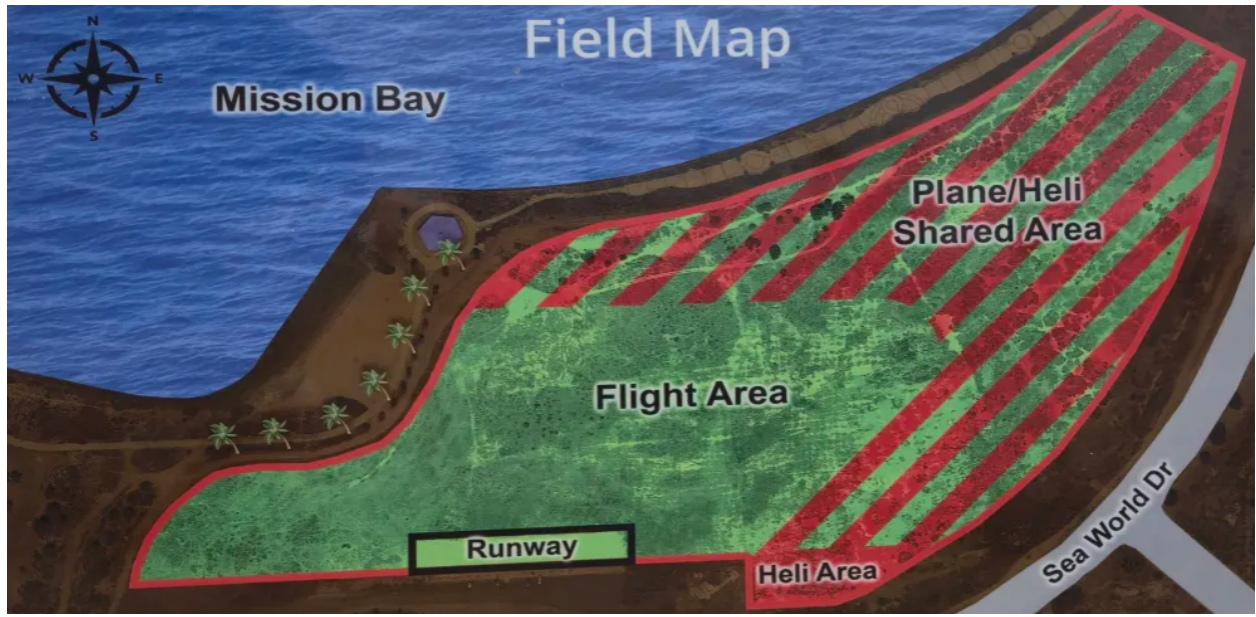
References

- [1] - Raymer, Daniel P. *Aircraft Design: A Conceptual Approach: A Conceptual Approach*. 6th ed., American Institute of Aeronautics and Astronautics Inc, 2018.
- [2] - *NACA 4412 (NACA4412-IL) Xfoil Prediction Polar at Re=1,000,000 Ncrit=5*, airfoiltools.com/polar/details?polar=xf-naca4412-il-1000000-n5. Accessed 19 Mar. 2025.
- [3] - Hwang, J.T, MAE 155B Lectures, University of California San Diego
- [4] - Hwang, J.T, MAE 155A Lectures, University of California San Diego
- [5] - <https://www.apcprop.com/technical-information/performance-data/>
- [6] - <https://www.cobramotorusa.com/motors-2217-16.html>
- [7] - https://www.amazon.com/dp/B07MC456T5?ref=ppx_yo2ov_dt_b_fed_asin_title&th=1

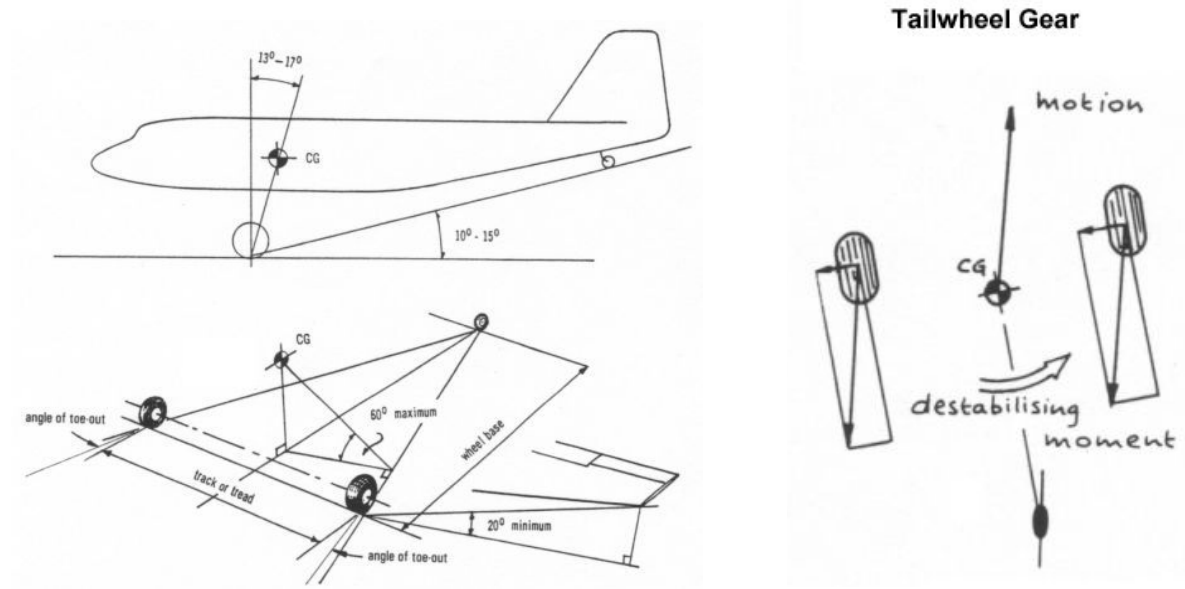
Appendices

Appendix A - Figures

A.3



A.5



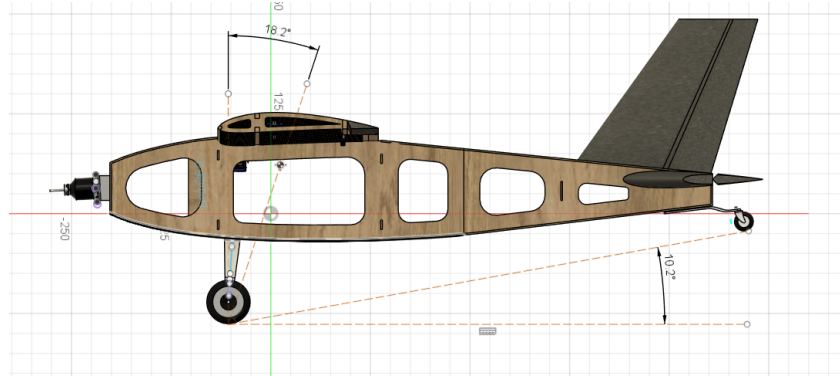


Figure A.5.1: The landing gear configuration (Tail dragger).

A.6

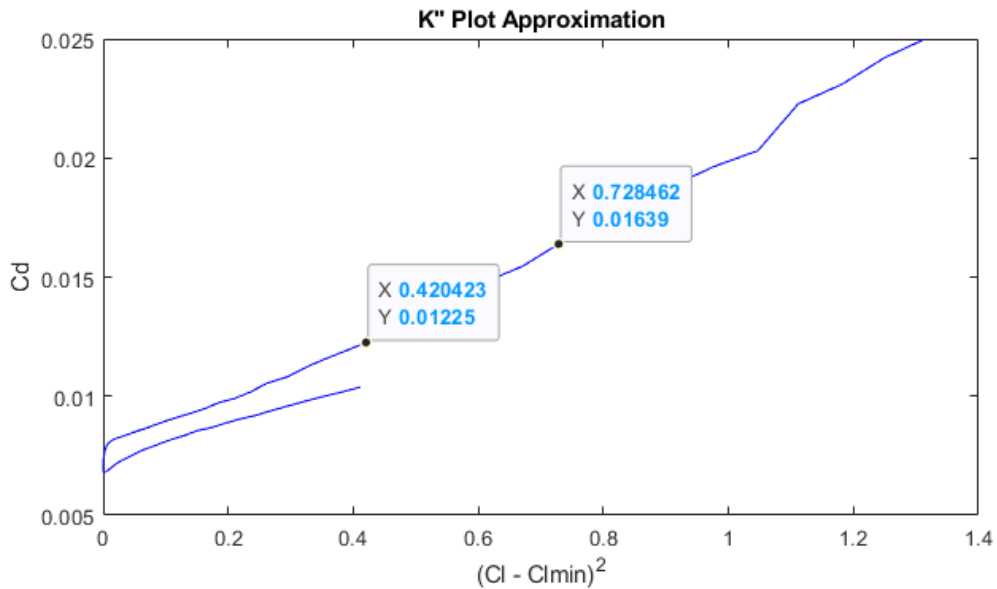


Figure A.6.1: K'' estimation from the 2-D aerodynamic data for 3-D aerodynamic data calculations in Figure 6.2.

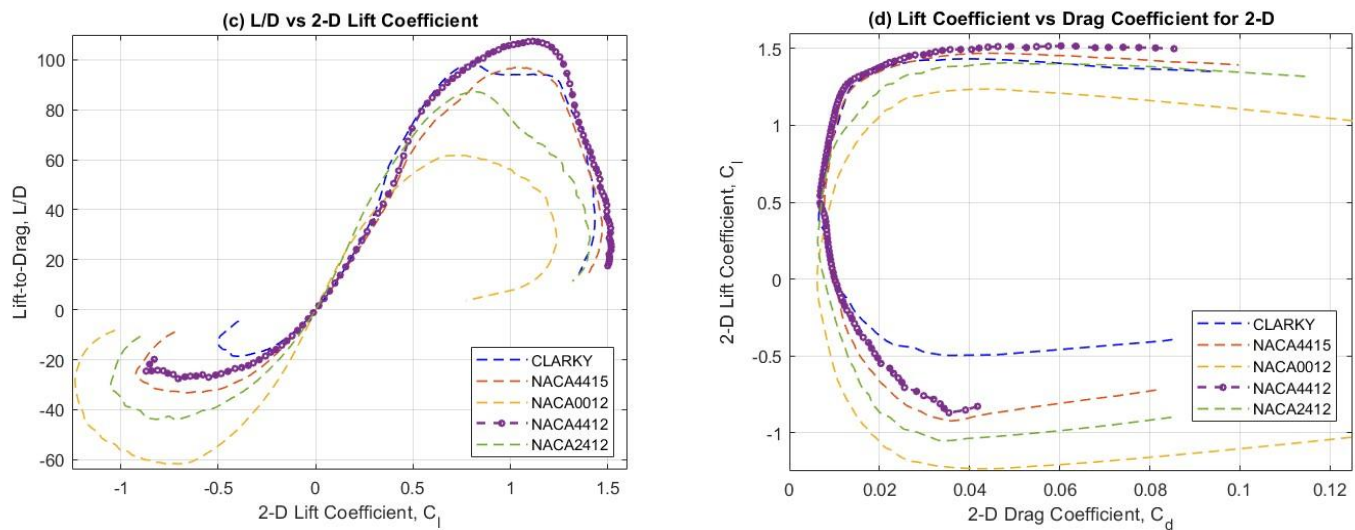


Figure A.6.2: Other 2-D aerodynamic data for selected airfoils at $Re = 500,000$. Data collected from XFOIL.

A.7

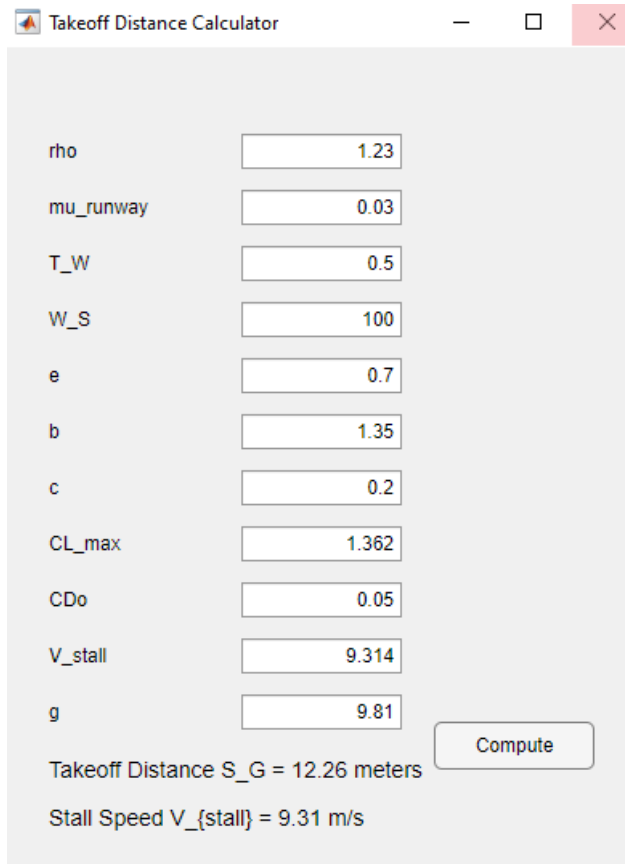


Figure A.7.1: The Graphical User Interface (GUI) of takeoff distance and stall speed calculations using MATLAB.



Figure A.7.2: Top View of Mission Bay Runway with approximate total runway distance (80m) using ArduPilot Mission Planner Software.

A.8

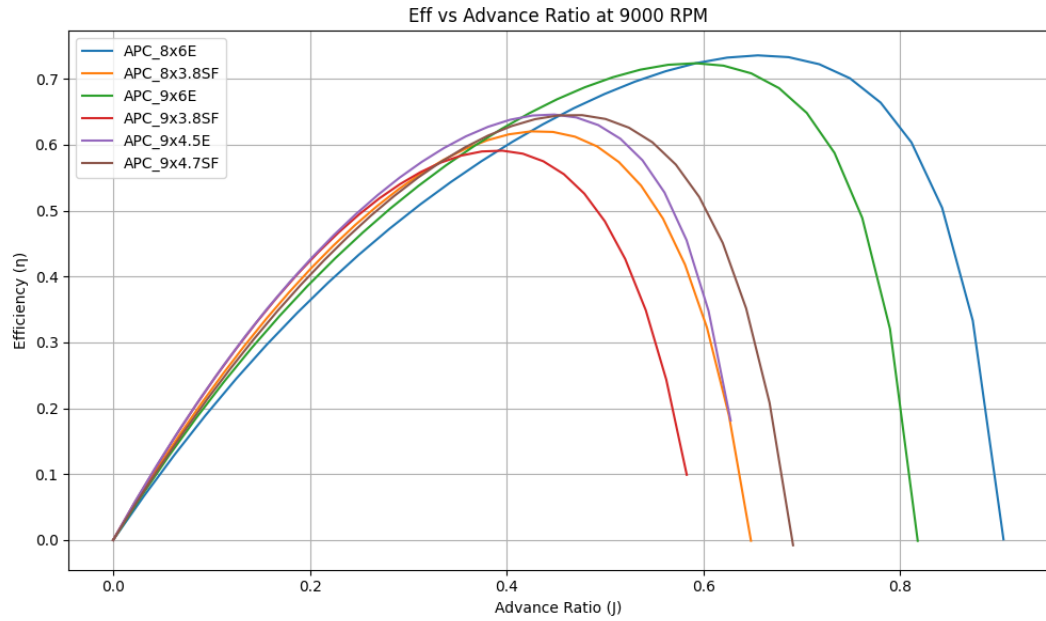


Figure A.8.1: Efficiency of different propellers as a function of advance ratio.

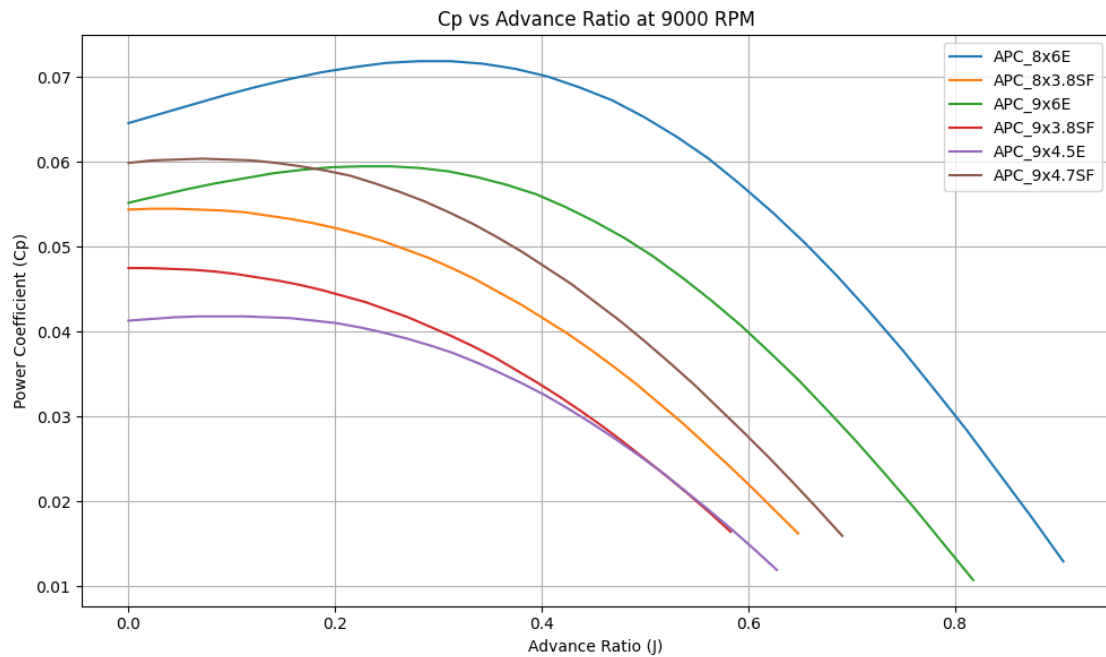


Figure A.8.1: Power coefficient of different propellers as a function of advance ratio.

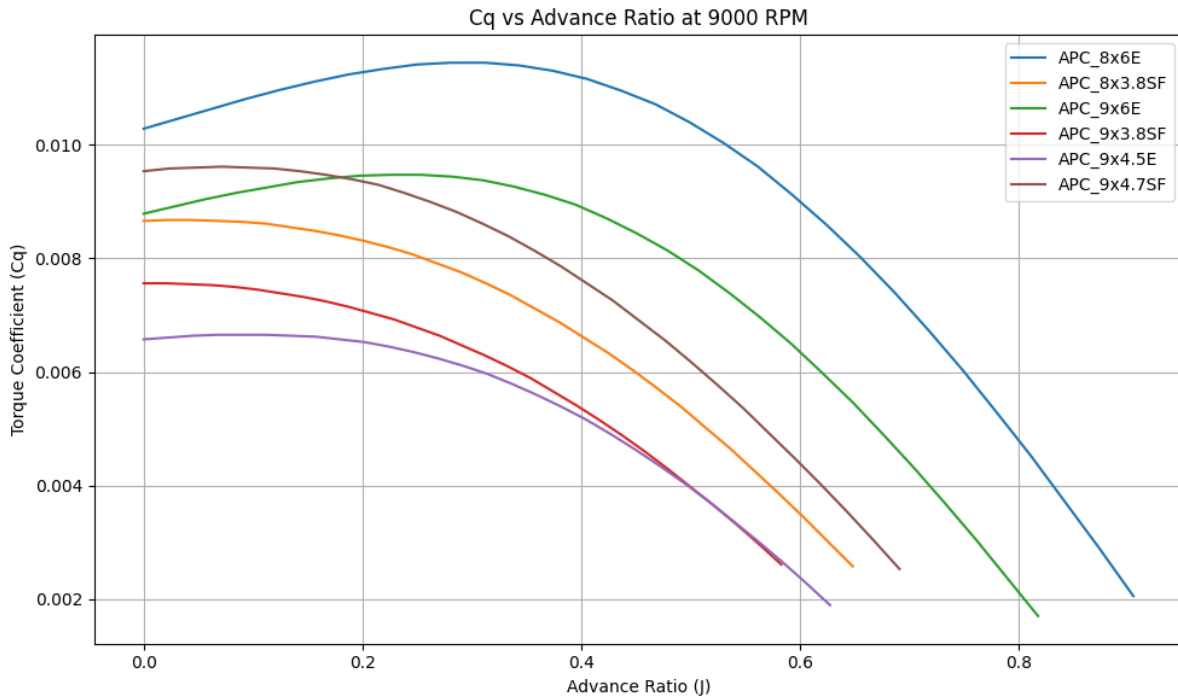


Figure A.8.2: Torque coefficient of different propellers as a function of advance ratio.

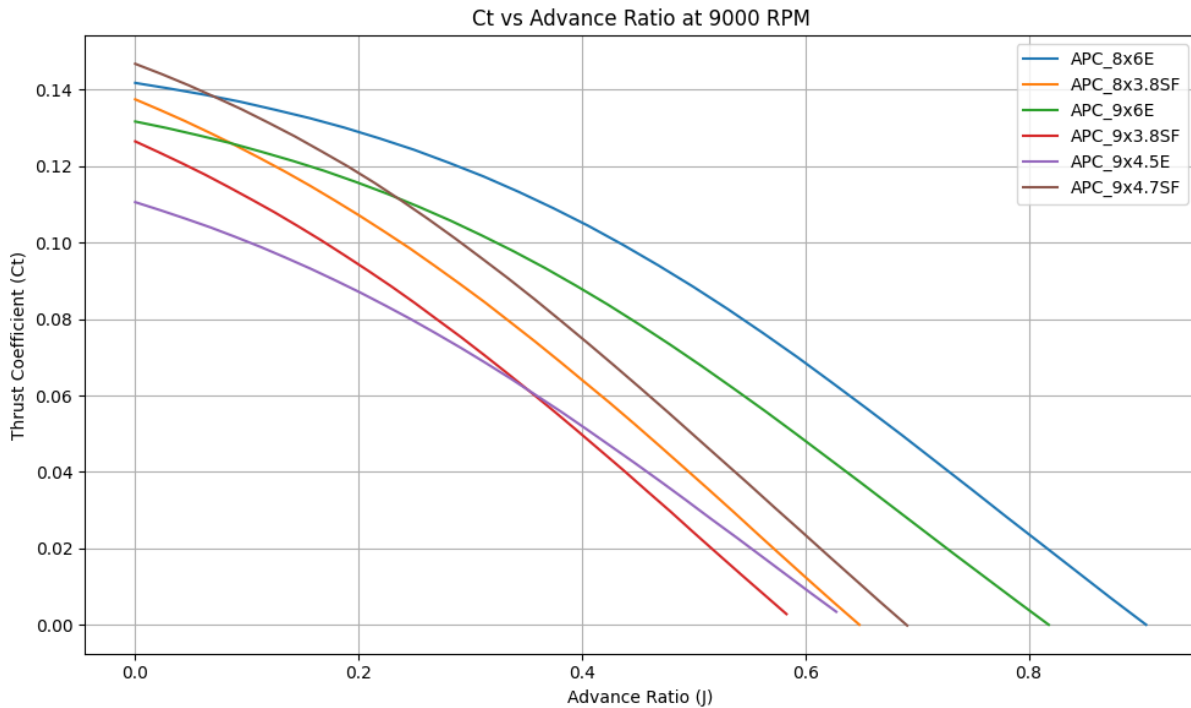


Figure A.8.3: Thrust coefficient of different propellers as a function of advance ratio.

A.9

	Typical values	
	Horizontal c_{HT}	Vertical c_{VT}
Sailplane	0.50	0.02
Homebuilt	0.50	0.04
General aviation—single engine	0.70	0.04
General aviation—twin engine	0.80	0.07
Agricultural	0.50	0.04
Twin turboprop	0.90	0.08
Flying boat	0.70	0.06
Jet trainer	0.70	0.06
Jet fighter	0.40	0.07–0.12*
Military cargo/bomber	1.00	0.08
Jet transport	1.00	0.09

Figure A.9.1: Image of table 6.4 from Raymer [1] textbook that lists typical Tail Volume Coefficients

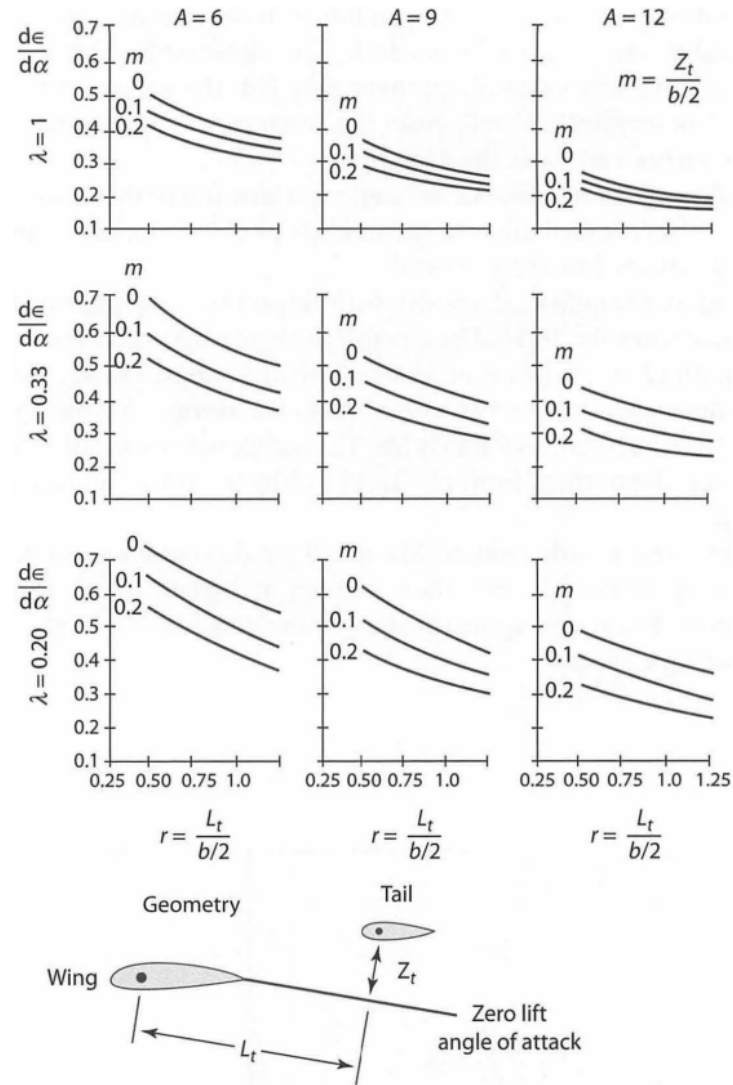


Figure A.9.2: Plots of different $\frac{d\epsilon}{d\alpha}$ vs r coefficient at varying taper, m coefficient, and aspect ratio.

A.10



Figure A.10.1.1: Top view of electronics bay showing the supporting brace for the main landing gear

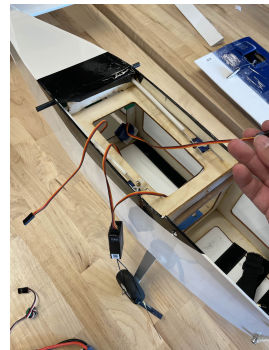


Figure A.10.1.2: Servo wiring in the fuselage

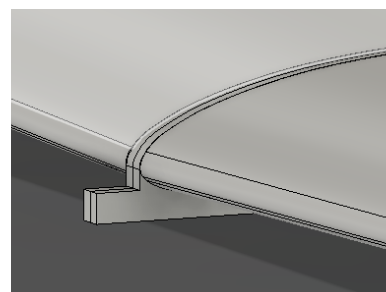


Figure A.10.1.3A: Center notch of the wing

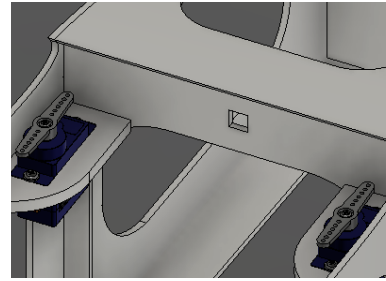


Figure A.10.1.3B: Hole for the notch to center the wing



Figure A.10.2.1: Construction of the wing showing the balsa spars and foam ailerons



Figure A.10.2.2: Servo mount for the aileron



Figure A.10.3.1: Top view of final horizontal and vertical tail design.



Figure A.10.3.2: Side view of final horizontal and vertical tail design.



Figure A.10.4.1: Top view of motor mount extension



Figure A.10.4.2: Motor mount extensions without the 3D printed brace



Figure A.10.4.3: Aluminum spacers

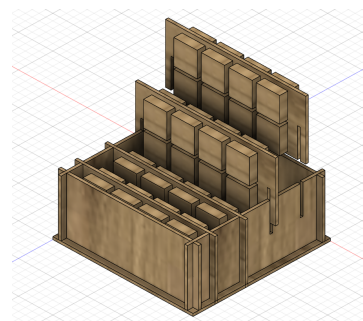


Figure A.10.5.1: Isometric view showing the payload weight slides



Figure A.10.5.2: Fabricated weight payload

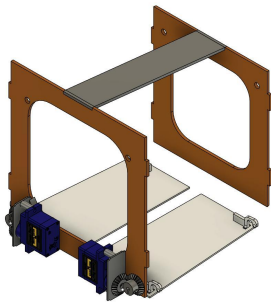


Figure A.10.6.1: CAD of payload drop-off mechanism

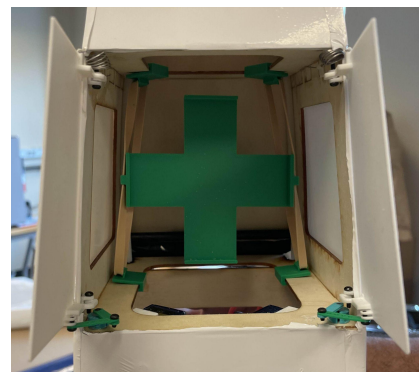


Figure A.10.6.2: Bottom view showing cargo bay doors opened and pusher

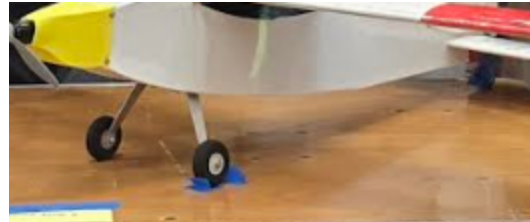


Figure A.10.7.1: Main landing gear



Figure A.10.7.2: Tail landing gear



Figure A.10.7.3: Tail landing gear side view



Figure A.10.8.1: Support Housing

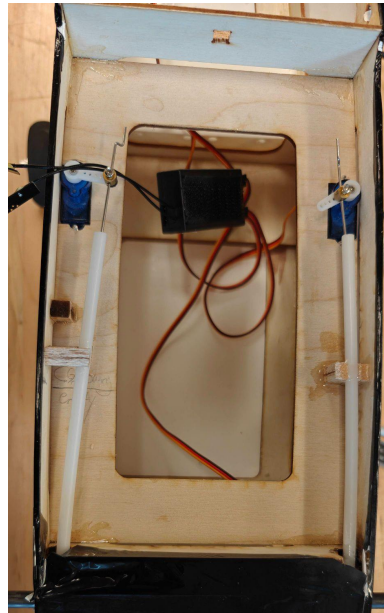


Figure A.10.8.2: Rear control configuration

Appendix B - Equations

B.4

B.4.1: Gross Weight Equation:

$$W_g = W_p + W_e + W_b$$

B.4.2: Scoring Function Equation

$$J(x) = \frac{r_{wp} W_p(x) + r_{vp} V_p(x) - c_e E_f(x) - c_c}{T_f(x)} - \frac{c_{wg} W_g(x)}{t_l} - c_f$$

B.5

B.5.1: Taildragger Landing Gear Equation

$$d_{forward} = h_{CG} x \tan(\theta)$$

B.6

B.6.1: Total Drag Coefficient Equation

$$C_D = C_{D,0} + \frac{C_L^2}{\pi \cdot e \cdot AR}$$

B.6.2: Drag Buildup — form and interference drag Equation

$$C_{D,0} = \frac{\sum (C_{fi} F F_i Q_i S_{wet_i})}{S_{ref}}$$

B.6.3: Reynolds Number Equation

$$Re = \frac{\rho V_{cruise} C}{\mu}$$

B.6.4: 3-D Maximum Lift Coefficient Equation

$$C_{L,max} = 0.9 C_{l,max} \cos(\Lambda_{c/4})$$

B.7

B.7.1-4: Aircraft Takeoff Distance Equations

$$\begin{aligned} K &= \frac{1}{\pi e AR} \\ K_T &= \left(\frac{T}{W} \right) - \mu \\ K_A &= \frac{\rho}{2(W/S)} (\mu C_L - C_{D,0} - KC_L^2) \\ S_G &= \left(\frac{1}{2gK_A} \right) \ln \left(\frac{K_T + K_A V_f^2}{K_T + K_A V_i^2} \right) \end{aligned}$$

B.7.5-6: Climb and Maneuvering Thrust to Weight Equations

$$\begin{aligned} \frac{T}{W} &\geq \sin(\gamma) + \frac{W/S}{\pi e AR q} + \frac{C_{D,0} q}{W/S} \\ \frac{T}{W} &\geq n^2 \frac{W/S}{\pi e AR q} + \frac{C_{D,0} q}{W/S} \end{aligned}$$

B.8

B.8.2: Aileron Area Equation

$$Aileron\ Area = Aileron\ Chord \times Aileron\ Span$$

B.8.2: Elevon Area Equation

$$\text{Elevon Area} = \text{Elevon Chord} \times \text{Elevon Span}$$

B.9

B.9.1: Horizontal and Vertical Tail Planform Area Equation

$$S_{HT} = \frac{c_{HT} C_W S_W}{L_{HT}}$$

$$S_{VT} = \frac{c_{VT} b_W S_W}{L_{VT}}$$

B.9.2: Center of Gravity Location Equation

$$x_{cg} = \frac{\sum_i W_i x_{cg,i}}{\sum_i W_i}$$

B.9.3: Horizontal Tail Lift Curve slope Equation

$$\frac{dC_{L,t}}{d\alpha} = \frac{dC_{L,t}}{d\alpha.t} \left(1 - \frac{d\varepsilon}{d\alpha}\right) \eta_h$$

B.9.4: Neutral Point Location formula

$$x_{np} = \frac{\sum_i \frac{dC_{L,i}}{d\alpha} S_i x_{ac,i}}{\sum_i \frac{dC_{L,i}}{d\alpha} S_i}$$

B.9.5: Static Margin Equation

$$SM = \frac{x_{np} - x_{cg}}{mac}$$

Appendix C - Tables

C.4

Revenue per unit payload weight	r_{W_p}	1
Revenue per unit payload volume	r_{V_p}	300
Cost per unit energy	c_e	0.3
(COC) Cost per flight	c_c	0.5
Cost per unit gross volume	c_{W_g}	300
(COF) Cost per unit flight-time	c_f	0.2
Total flight time in aircraft life	t_l	1000

Table C.4.1: Scoring Function's fixed parameter values

Gravitational Acceleration	g	9.81 [m/s ²]	Given (Earth's Gravity)
Battery Parameters	n_b	0.85	Assumption
	e_b	453069.786	= (11.1 v)(1.8 Ah)(3600 J/Wh)/(0.158757 kg)
Flight Range	R_{flight}	600 [m]	Provided in <i>Table 1.1</i>
Lift-to-Drag Ratio	L/D	8-13	Assumption
	$Tf(x)$	—	= 20*R_flight / 3600*V_cruise
Require Thrust to maintain cruise	Thrust_req_cruise	—	= 4.4482216153 * (1 / (L/D)) * W_g
Power	P_{in}	—	= Thrust_req_cruise*V_cruise/1000
	$E_f(x)$	—	= (20*P_in/n_b) * (R_flight/3600*V_cruise)
Known Weight	W_{known}	0.8642 [lb]	Given (Component Weights)
Airframe Weight	W_{airframe}	2.0358 [lb]	= W_g - W_known - Wp(x)
Empty Weight	W_e	2.9 [lb]	= W_known + W_airframe
	W_e/W_g	0.66	= W_e/W_g
Gross Weight	W_g	4.4 [lb]	Assumption
Cruise Speed	V_{cruise}	25 [m/s]	Assumption
Payload Weight	W_p	1.5 [lb]	Assumption

Table C.4.2: Scoring Function's Parameter Assumptions and Values

From the student-built aircrafts' reference sizing values:

Wing Loading	W/S	100 N/m ²
Thrust-to-weight	T/W	0.8

Utilized to make initial assumptions for:

Gross Weight	W_g	4.4 lb
Wing Area	A	0.27 m ²

Table C.4.3: Assumptions on initial gross weight and wing area based on student-built aircrafts (MAE 155B)

C.5

FIXED COMPONENT

Transmitters	RotorLogic RadioMaster TX16S
Batteries	Tattu 11.1V 1800mAh 3S 45C LiPo
Motor	Cobra C-2217/16 Brushless, Kv=1180 ¹
Speed controller	40 Amp ESC ²
Receivers	FrSky Taranis Receiver X8R 8 Channel
Servos	Smraza 10 Pcs SG90 9G Micro Servo
Servo extensions	30 Pcs 3-Pin Extension Cable
Servo linkages	Pushrod, 16.5" ³ Linkage stoppers ⁴ Control horns ⁵
Some battery monitor	Treat like another battery in size/volume
Landing gear	Aluminum landing gear set—Cessna 182 Parts

Table C.5.1: List of the fixed components and available components

MATERIALS & DESCRIPTIONS

Wing spar	Flat carbon fiber, 1 x 6 x 1000 mm Circular tube, 0.32"/0.25" outer/inner diameter, 60" long ⁶
Epoxy glue	BSI-201 Quik-Cure Epoxy
Rubber bands	—
Nuts / bolts	M5 x 6mm/8mm/10mm
Tail boom	Circular tube, 0.715"/0.625" outer/ inner diameter, 70" long ⁷
Foam boards	— ⁸
Balsa sheets	1/16" thick, 8" x 12"
Balsa sticks	Square section, 1/8", 12" long
Fasteners	Cable straps and cable ties

Table C.5.2: List of the available parts and materials

¹ [Cobra C-2217/16 Brushless Motor, Kv=1180](#)² [Amazon.com: Flycolor 40A ESC 2-4S Electric Speed Controller 5v 3A BEC with XT60 & 3.5mm Bullet Plugs for RC Drone Airplane Brushless Motors : Toys & Games](#)³ [16.5" Push Rods \(8-Pack\) | RC Plane Building Materials | Flite Test](#)⁴ [Quick-Connect Linkage Stoppers \(6-Pack\) | RC Plane Building Materials | Flite Test](#)⁵ [FT Control Horn \(20 pieces\) | RC Plane Building Materials | Flite Test](#)⁶ [Carbon Fiber Roll Wrapped Tube, 0.320"OD](#)⁷ [Carbon Fiber Roll Wrapped Tube, 0.711"OD](#)⁸ [Elite Test Retail Store - Not Found](#)

MATERIALS & DESCRIPTIONS

Velcro	16' long, 0.75" wide strips
Hinges	11x25.5 mm 0.43" x1.0"
Hardwood blocks	1"~4" blocks, maple, cherry, walnut
Plywood	1/8" x 12" x 24" birch plywood
Basswood	1/16" x 12" x 8" basswood sheets
Foam	2" x 4' x 8' 25 PSI blue foam
Monokote	White, yellow, blue
Sandpaper	—
Duct tape	—
Vinyl/plastic gloves	—
GPS speed tracker	SKYRC GSM-015

Table C.5.3: List of the other available parts and materials

PROPELLER

b9x6sf⁹	11x8e¹⁰
b9x9e¹¹	b12x6e¹²
b9x7-5e¹³	b12x8e¹⁴
10x7e¹⁵	13x8e¹⁶
10x10e¹⁷	13x6-5e¹⁸

Table C.5.4: List of the propeller choices

C.6

Part	Cf	FF	Q	Swet/Sref	C _{D0} (Raymer)
Wing Section	0.0023	1.0521	1.1	2.047957	0.0054
Fuselage	0.0023	1.2347	1.1	From code	0.0063
Landing Gear	0.0023		1.1	From code	0.0057
Motor	0.0023		1.1	From code	0.019
		Total			0.0364

Table C.6.1: Drag buildup for the 3D drag aerodynamic analysis

⁹ [B9x6SF - APC Propellers](#)

¹⁰ [11x8E - APC Propellers](#)

¹¹ [B9x9E - APC Propellers](#)

¹² [b12x6E - APC Propellers](#)

¹³ [B9x7.5E - APC Propellers](#)

¹⁴ [b12x8E - APC Propellers](#)

¹⁵ [10x7E - APC Propellers](#)

¹⁶ [13x8E - APC Propellers](#)

¹⁷ [10x10E - APC Propellers](#)

¹⁸ [13x6.5E - APC Propellers](#)

C.8

SPECIFICATIONS		BRUSHLESS MOTOR Cobra C-2217/16
Weight [kg]		73.0 grams
Size [mm]		mm (diameter) x mm (thickness)
Max Power [W]		265 Watts
Max Thrust [kg]		—
Max Amp [A]		24 Amps
KV rating		1180
ESC		—

Table C.8.1: Specifications of the required brushless motor.¹⁹

SPECIFICATIONS	BATTERY [Tattu]
Weight [kg]	158g
Size [mm]	106*35.5*21mm Tattu 11.1V 1800mAh 3S 45C LiPo Battery Pack
Voltage [V]	11.1 Volts
Energy density	200Wh/kg energy density

Table C.8.2: Specifications of the required battery²⁰.

¹⁹ [Cobra C-2217/16 Brushless Motor, Kv=1180](#)

²⁰ [Amazon.com: Tattu 11.1V 1800mAh 3S 45C LiPo Battery Pack with XT60 Plug for Skylark M4-FPV250 Mini Shredder 200 INDY250 PLUS MOJO 280 QAV250 Vortex Emax Nighthawk 250 RC Heli Airplane UAV Drone FPV : Toys & Games](#)

FIXED COMPONENT	BATTERY Tattu
Transmitters	RotorLogic RadioMaster TX16S
Batteries	Tattu 11.1V 1800mAh 3S 45C LiPo
Motor	Cobra C-2217/16 Brushless, Kv=1180 ²¹
Speed controller	40 Amp ESC ²²
Receivers	FrSky Taranis Receiver X8R 8 Channel
Servos	Smraza 10 Pcs SG90 9G Micro Servo
Servo extensions	30 Pcs 3-Pin Extension Cable
Servo linkages	Pushrod, 16.5" ²³ Linkage stoppers ²⁴ Control horns ²⁵
Landing gear	Aluminum landing gear set—Cessna 182 Parts Replacement 40 Size ARF PNP

Table C.8.3: List of the fixed components and available components

PROP SIZE	PROP RPM
APC 8x3.8-SF	10,250
APC 8x6-E	9,790
APC 9x3.8-SF	9,560
APC 9x6-E	9,450
APC 9x4.5-E	9,860
APC 9x4.7-SF	9,684

Table C.8.4: List of the propeller size choices and corresponding RPMs.

²¹ [Cobra C-2217/16 Brushless Motor, Kv=1180](#)

²² [Amazon.com: Flycolor 40A ESC 2-4S Electric Speed Controller 5v 3A BEC with XT60 & 3.5mm Bullet Plugs for RC Drone Airplane Brushless Motors : Toys & Games](#)

²³ [16.5" Push Rods \(8-Pack\) | RC Plane Building Materials | Flite Test](#)

²⁴ [Quick-Connect Linkage Stoppers \(6-Pack\) | RC Plane Building Materials | Flite Test](#)

²⁵ [FT Control Horn \(20 pieces\) | RC Plane Building Materials | Flite Test](#)

C.9

Component Name	X _{CG} (m) distance from Fuselage Nose	Mass (g)
APC 9x6E Propeller	-0.055	18.8
Cobra 2217/16 Motor	-0.04	76.3
Watt Meter	0.05	91.4
40a ESC	0.05	52
Battery	0.05	144.3
Nose Cone	-0.03	38.3
Front Landing Gear	0.13	54.1
Payload 1	0.175	681
Wing	0.18	330
Payload 2	0.24	33
Fuselage Structure	0.33	484.6
Tail Structure	0.6	50
Rear Landing Gear	0.8	28.2
Empty Weight		1401
Total		2082

Table C.9.1: List of individual component's mass and center of gravity location from fuselage structure nose along X axis.

PARAMETERS	VALUE
Wing Lift Curve Slope ($\frac{dC_{L,W}}{d\alpha}$)	6.0752 rad ⁻¹
Tail Lift Curve Slope ($\frac{dC_{L,T}}{d\alpha,T}$)	6.3 rad ⁻¹
Downwash-Angle Derivative ($\frac{d\varepsilon}{d\alpha}$)	0.46
Tail Efficiency Factor (η_h) [3]	0.9
Tail Lift Curve Slope ($\frac{dC_{L,T}}{d\alpha}$)	3.0618 rad ⁻¹

Table C.9.2: Aerodynamic parameters used to calculate Neutral point

Cobra C2217/16 Motor Propeller Data									
Motor Wind 16-Turn Delta		Motor Kv 1180 RPM/Volt		No-Load Current $I_0 = 0.75$ Amps @ 8V		Motor Resistance $R_m = 0.070$ Ohms		I Max 24 Amps	P Max (3S) 265 W
Prop Manf.	Prop Size	Input Voltage	Motor Amps	Watts Input	Prop RPM	Pitch Speed	Thrust Grams	Thrust Ounces	Thrust Eff. Grams/W
APC	8x3.8-SF	11.1	13.75	152.6	10,250	36.8	839	29.59	5.50
APC	8x4-E	11.1	11.59	128.6	10,610	40.2	719	25.36	5.59
APC	8x6-E	11.1	16.70	185.4	9,790	55.6	832	29.35	4.49
APC	8x6-SF	11.1	21.16	234.9	9,000	51.1	872	30.76	3.71
APC	8x8-E	11.1	21.15	234.8	9,010	68.3	728	25.68	3.10
APC	9x3.8-SF	11.1	17.78	197.4	9,560	34.4	1068	37.67	5.41
APC	9x4.5-E	11.1	16.10	178.7	9,860	42.0	998	35.20	5.58
APC	9x4.7-SF	11.1	17.07	189.5	9,684	43.1	1050	37.04	5.54
APC	9x6-E	11.1	18.63	206.8	9,450	53.7	1058	37.32	5.12
APC	9x6-SF	11.1	26.94	299.0	7,930	45.1	1081	38.13	3.61
APC	9x7.5-E	11.1	23.84	264.6	8,560	60.8	1036	36.54	3.91
APC	10x3.8-SF	11.1	25.08	278.4	8,250	29.7	1314	46.35	4.72
APC	10x5-E	11.1	21.11	234.3	9,000	42.6	1166	41.13	4.98
APC	10x6-E	11.1	22.19	246.3	8,770	49.8	1224	43.17	4.97
APC	10x7-E	11.1	24.67	273.8	8,320	55.2	1217	42.93	4.44
APC	11x5.5-E	11.1	25.89	287.4	8,114	42.3	1383	48.78	4.81
GWS	8x4-DD	11.1	9.14	101.5	11,020	41.7	656	23.14	6.47
GWS	9x5-DD	11.1	15.60	173.2	9,920	47.0	994	35.06	5.74
GWS	9x5x3-DD	11.1	19.39	215.2	9,330	44.2	1096	38.66	5.09
GWS	10x6-DD	11.1	20.11	223.2	9,190	52.2	1162	40.99	5.21
GWS	10x6x3-DD	11.1	24.39	270.7	8,400	47.7	1322	46.63	4.88

Table C.9.3: List of various off shelf propellers for Cobra C2217 motor at set 11.1 input voltage.

[5]

